Universidade de Aveiro
2020
Departamento de Engenharia de Materiais e Cerâmica

Sara Diana Gomes Carvalho

Estruturas 3D grafeno/matriz biológica estimuláveis mecanicamente para engenharia de tecido ósseo

Mechanical stimulus responsive 3D-Bio based graphene scaffolds for bone tissue engineering

Sara Diana Gomes Carvalho

Mechanical stimulus responsive 3D-Bio based graphene scaffolds for bone tissue engineering

Dissertação apresentada à Universidade de Aveiro para cumprimento dos requisitos necessários à obtenção do grau de Mestre em Materiais e Dispositivos Biomédicos, realizada sob a orientação científica do Doutor Gil Gonçalves, investigador do Centro de Tecnologia Mecânica e Automação (TEMA) da Universidade de Aveiro e coorientação científica da Doutora Paula Marques, investigadora do Centro de Tecnologia Mecânica e Automação (TEMA) da Universidade de Aveiro.

o júri

presidente

Professor Doutor Augusto Luís Barros Lopes
Professor Auxiliar da Universidade de Aveiro

Doutora Paula Celeste da Silva Ferreira
Investigadora Coordenadora em Regime Laboral da Universidade de Aveiro

Doutor Gil Alberto Batista Gonçalves
Equiparado a Investigador Auxiliar da Universidade de Aveiro

agradecimentos

A escrita da tese de mestrado, apesar de ser um processo solitário a que qualquer investigador está destinado reúne contributos de várias pessoas. Daí, o meu profundo e sentido agradecimento a todas as pessoas que contribuíram para a concretização desta dissertação, estimulando-me intelectual e emocionalmente.

Ao Doutor Gil Gonçalves, que se mostrou sempre disponível para ajudar e contribuir para que o trabalho realizado se tornasse o melhor possível.

À Doutora Paula Marques pela sua disponibilidade e por se mostrar interessada em todo o processo laboratorial.

Aos colegas e investigadores do TEMA que de algum modo me ajudaram a superar os problemas que surgiram e me apoiaram e partilharam os seus conhecimentos comigo. Um agradecimento especial à Ângela Sêmitela e à Andreia Leal, por toda a ajuda, disponibilidade, encorajamento e amizade nestes meses de incerteza. Obrigada à Catarina, que estando na mesma situação que eu, se tornou num pilar nesta jornada de aprendizagem. Obrigada à minha família, à minha mãe, irmão, Andreia e Daniel pela ajuda emocional que me deram, mesmo nas alturas menos boas do decorrer da dissertação.

Aos meus amigos, que viram o tempo de partilha diminuído, estando sempre presentes.

Um especial agradecimento à Bone Easy e à Sunlive, pela disponibilidade e apoio para que conseguisse concretizar as minhas metas e acreditarem em mim.

palavras-chave Óxido de grafeno; Diferenciação; células estaminais; Scaffolds; Engenharia de Tecidos; Estimulação; organismos marinhos; Biocompatibilidade; Regeneração óssea

resumo

A engenharia de tecido ósseo ganhou grande relevância nos últimos anos devido ao potencial de gerar tecido funcional. Na regeneração do tecido ósseo, são várias as opções que podem ser adotadas, sendo a substituição óssea autóloga o procedimento clínico preferencial. No entanto, a limitada quantidade disponível de materiais autólogos no corpo, leva a que esta opção seja pouco utilizada. Como alternativas, tem havido esforços significativos no desenvolvimento de materiais sintéticos para incorporação nos pacientes, de modo a restaurar a forma e função do osso lesado.

O foco deste trabalho foi o desenvolvimento de biomateriais para regeneração óssea, os quais devem possuir características biológicas específicas relevantes para que sejam incorporados no corpo humano. Estes devem mimetizar a estrutura e função da matriz extracelular (ECM) do osso, a fim de fornecer um ambiente tridimensional (3D) capaz de melhorar a adesão, proliferação e diferenciação celular, assim como possuir características biofísicas e bioquímicas adequadas para induzir e potencializar a regeneração do tecido ósseo. Atualmente, os biomateriais obtidos de fontes naturais são opções promissoras para aplicação em engenharia de tecidos devido ao seu bom desempenho biológico.

Neste trabalho foi realizado pela primeira vez o self-assembly de óxido de grafeno (GO) numa matriz de espongina natural (MS) pelo método camada a camada (do inglês *layer-by-layer* (LbL)). As propriedades mecânicas e biológicas resultantes da modificação da MS tornam-na uma candidata muito relevante para explorar como um modelo no desenvolvimento de novos suportes biomiméticos com características estruturais e bioquímicas adequadas para células ósseas. Inicialmente, este trabalho foi dedicado à purificação da MS no que diz respeito à remoção de alguns constituintes anatómicos ou contaminantes. A composição química, estrutura e propriedades mecânicas da MS foram avaliadas por meio de testes de FTIR, SEM e compressão mecânica. A preparação dos bionanocompósitos foi realizada analisando o self-assembly do GO na superfície da MS utilizando diferentes polieletrólitos positivos (PDDA e PEI). Os resultados obtidos mostraram que a deposição de multicamadas GO / PEI dá origem a uma funcionalização superficial altamente eficiente da MS. Estes materiais híbridos apresentaram elevada estabilidade mecânica e térmica, o que permite a preparação de dois conjuntos de amostras com GO reduzido (rGO) e não reduzido, para o desenvolvimento de estudos biológicos. Os estudos *in vitro* realizados com osteoblastos em condições dinâmicas revelaram que os bionanocompósitos preparados com GO apresentaram melhor desempenho em termos de viabilidade e mineralização celular. Esses resultados podem ser atribuídos principalmente ao fato de o GO apresentar mais grupos funcionais contendo oxigénio na sua composição do que o rGO. Estes bionanocompósitos foram capazes de promover a adesão e proliferação celular e, mais importante, garantir a sua integridade estrutural durante o teste dinâmico.

keywords

Graphene oxide; Differentiation; stem cells; Scaffolds; Tissue Engineering; Stimulation; marine organisms; Biocompatibility; Bone regeneration

abstract

Bone tissue engineering has gained a high relevance in the past few years due to the potential to generate functional tissue. In bone tissue regeneration, there are several options that can be adopted, being the autologous bone replacement the preferential clinical procedure. However, the use of autologous materials has a drawback that consists of the limited quantity available in the body. As alternatives, significant efforts have been dedicated to developing synthetic materials for the incorporation in the patients to restore the form and function of the injured bone.

This work focus on the development of biomaterials for bone regeneration, which must possess relevant specific biological characteristics to be incorporated into the human body. They must mimic the function and structure of the bone extracellular matrix (ECM), in order to provide a three-dimensional (3D) environment capable of improving cellular adhesion, proliferation and differentiation, as well as presenting adequate biophysical and biochemical characteristics to induce and potentiate the bone tissue regeneration. Currently, biomaterials obtained from natural sources are promising options for application in tissue engineering due to their good biological performance.

In this work, it was reported for the first time the self-assembly of graphene oxide (GO) nanosheets on the natural spongin skeleton by the layer-by layer (LbL) method. These improved mechanical and biological properties of the MS make it a very relevant candidate to explore as a template for the development of new biomimetic scaffolds with appropriate structural and biochemical cues for bone cells. Firstly, this work was dedicated to the MS purification regarding the removal of some anatomic constituents or contaminants. The chemical composition, structure and mechanical properties of MS were accessed, by FTIR, SEM and mechanical compression tests. The preparation of the bionanocomposites was performed by exploring the self-assembly of GO on the surface of MS using different positive polyelectrolytes (PDDA and PEI). The obtained results showed that the multilayer deposition PEI/GO gives rise to highly efficient surface functionalization of MS. These hybrids materials showed a high mechanical and thermal stability, which allows the preparation of two sets of samples, with reduced(rGO) and non-reduced GO, for the development of biological studies. The *in vitro* studies performed with osteoblasts under dynamic conditions revealed that the bionanocomposites prepared with GO showed an improved performance in terms of cell viability and mineralization. These results can be mainly attributed to the fact that GO presents more oxygen functional groups in its composition than the samples with rGO. These bionanocomposites were able to promote cell adhesion and proliferation, and more importantly guaranty their structural integrity of during the dynamic test.

Índice

Abbreviations list

ECM	Extracellular matrix
TE	Tissue Engeneering
MS	Spongin Skeleton of Marine Sponge
GBM	Graphene-Base Materials
GO	Graphene Oxide
PolyP	Polyphosphate
PEI	Polyethyleneimine
PDDA	Poly(diallyldimethylammonium chloride
CT	Computed Tomography
FTIR	Fourier transform infrared spectroscopy r
SEM	Scanning Electron Microscopy
MSH2O	Marine sponge washed with water
TGA	Thermogravimetric Analysis
rGO	Reduced Graphene Oxide
MS/GO	Marine sponge covered with GO
MSHCl	Marine sponge washed with Hydrochloric acid
HCl	Hydrochloric acid
PEI/GO	Marine sponge covered by PEI and GO by LbL
PDDA/GO	Marine sponge covered by PDDA and GO by LbL
PEI/rGO	Marine sponge covered by PEI and GO by LbL after thermal treatment
MSTT	Marine sponge thermal treated
CVD	Chemical Vapour Deposition

Figures List

List of Tables

CHAPTER 1

1. Introduction

1.1. Project Framework and Presentation

In bone tissue regeneration, there are several options that can be adopted, being the autologous bone replacement as the preferential clinical procedure. Because of limited quantity available in the body, the autologous materials cannot be used as a chosen method for every case. As alternatives, the development of synthetic materials for the incorporation in the patients is very important to restore the form and function of the injured bone. These materials are usually designated as biomaterials and should possess relevant specific biological and structural features in order to result in the best outcome, when incorporated in human body[1]. The main goal of the biomaterials is to mimic the structure and function of the natural bone extracellular matrix (ECM), in order to provide a three-dimensional (3D) environment to improve cell adhesion, proliferation, and differentiation[2]. Besides, biomaterials should possess adequate biophysical and biochemical features to induce and enhance the tissue repair. The main issues in bone tissue engineering (TE) are: 1) the biocompatibility of the scaffold which closely mimics the natural bone extracellular matrix, 2) osteogenic cells that incorporate the bone tissue matrix and 3) the ability for sufficient vascularization to allow the necessary tissue nutrient supply in the region[3,4]. Currently, materials obtained from natural sources have become relevant options for TE applications due to their large availability, easy to process and improved biological performance[4].

The materials of natural origin have become an important source for the development of novel scaffolds for bone tissue engineering, since generally they present superior biocompatibility and bioactivity[4]. Their assembly and further engineering allow the development of a large multitude of advanced supporting materials with many different architectures and features beneficial for bone tissue

growth. Hippospongia communis (Demospongiae, Dictyoceratida, Spongiidae), also known as “honeycomb’ sponge is one of the most abundant and with high commercial value in the marine sponge market, currently being mass harvested throughout the Mediterranean Sea[5]. Its structure is mainly composed by biossilica, polyphosphates and an analogous protein of animal collagen fibres designated as spongin. The 3D structure of the spongin matrix (MS) provides relevant mechanical and biocompatibility properties for the culture of osteogenic cell lines[2,5].

Graphene-based materials (GBM) are well known by having high biocompatibility, high surface chemical diversity and remarkable electronic and mechanical properties[6]. These features make GBM as excellent candidates to promote bone tissue regeneration. In this context, GBM had been widely explored on the development of smart scaffold materials able to provide biophysical and biochemical stimulus to induce the cell behaviour[7–11]. In terms of bone regeneration, it was highlighted the capacity of GBM to induce the differentiation of stem cells to osteogenic cells lines, under mechanical stimulation[7]. Eventhough, it has been suggested that elastic properties of GBM are the main responsible feature to trigger mechanosensitive pathways that promotes cell osteogenic differentiation[6]. However, the real mechanisms involved remain largely unknown. In this work, graphene oxide (GO) will be used as a starting nanomaterial for the coverage of the MS in order to enhance its biocompatibility and the result material will be heat treated to allow different reduction degrees of GO and its influence in the cells behaviour[6].

The methodology to modify the surface of the MS with GBM will consist in the use of the layer-by-layer (LbL) technique, that is considered one of the most simple and versatile approach for the controlled fabrication of single or multilayer thin films. The composition, thickness and architecture of these coatings can be precisely controlled using the combination of oppositely-charged polyeletrolytes[12,13]. As both MS and GBM are negatively charged, a positive polyeletrolyte, such as chitosan, polyamide, poly(diallyldimethylammonium chloride) (PDDA) and polyethyleneimine (PEI) needs to be used in order to promote the establishment of stable electrostatic interactions[12,13].

1.2. Objetives

This work intents to explore different synthetic strategies for the development of smart biomimetic MS/GBM scaffolds, aimed to be able to provide chemical, physical and topographical indicators to the osteoblastic cells during *incubation* under dynamic conditions in a bioreactor in order to improve cell adhesion and proliferation. For that purpose, it is intended that MS matrix will be carefully purified and characterized in terms of chemical and mechanical structure. The modification of the MS matrix will be employed through the surface modification with GBM using LbL approach, by exploring the combination of diverse polyelectrolytes and assembly strategies. Several studies will be dedicated to optimizing and validate the structural integrity of the MS/GBM scaffolds by applying different mechanical loads conditions under wet and dry state. After the first screening, the optimized scaffolds will be evaluated *in vitro* regarding their biocompatibility and their ability to induce cell proliferation and mineralization under static and dynamic mechanical stimulation in an osteoblastic cell culture.

CHAPTER 2

2. Bibliographic Revision

2.1. Bone structure and regeneration

Bone is known as a calcified extracellular matrix (ECM), being the main constituent of human skeleton. Its main functions are mechanical, making the structure of the body, support its weight and is directly linked to the movement. Besides, its metabolic functions, allows to produce cellular elements of blood and protect the integrity of intern organs[14]. It is always in continuous renewal, being a reserve of ions such as calcium and phosphate. This exchange of matrix is the result of the balance of mainly two types of cells: osteoclasts that absorb the calcified matrix and osteoblasts that synthesize new bone matrix[15–17]. Bone tissue can be divided in two categories: 1) cortical bone, that is the thick outer surface of a long bone, being compact and providing strength to all bones of the body, contributing for about 80% of the total human skeleton; and 2) trabecular or spongy bone, that is less dense than the cortical one, softer and weaker bone tissue with higher surface area. This bone tissue is highly vascular and frequently contains red bone marrow, where blood cells are formed[15–17]. Because of the different characteristics, their mechanical properties are distinct too, as shown on Table 1.

Table 1. Mechanical properties of bone tissue.[1,17]

Bone tissue	Tensile strength (MPa)	Compressive strength (MPa)	Young's Modulus (GPa)	Tenacity (MPa m $^{1/2}$)
Cortical Bone	60-160	130-180	3-30	2-12
Trabecular Bone	7,4	4-12	0,02-0,02	--

Bone tissue has three different components that make its structure (Figure 1). A thin membrane that surrounds the bone called the periosteum. It contains connective tissue with several blood vessels and nerves. Bone tissue also presents a dense structure defined as compact bone and is composed by both,

organic and inorganic phases. Collagen I is the main component in this organic phase (about 90% of organic matrix) with structural function that allows simultaneously flexibility and elasticity due to its fibrous complex structure. Hydroxyapatite represents the major fraction of the inorganic phase of the bone, being responsible by bone's toughness and resistance to shock[17]. In the internal layer of the bone, there is a sponge-like material named bone marrow. It is a gelatinous tissue that produces all blood cells, like red blood cells, white blood cells, platelets, osteoblasts, osteoclasts and fibers[17].

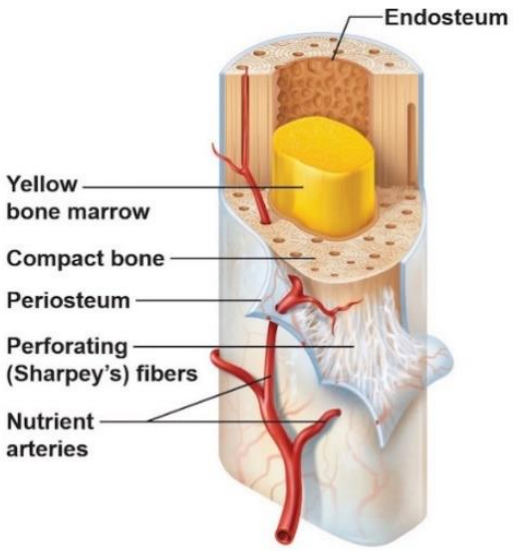

Figure 1. Schematic representation of bone structure.

When a fracture or damage occurs, bone reacts with a healing process in order to restore the tissue with its original properties and functions. This biological mechanism can be defined in three main different stages. The inflammatory stage, where the fractured zone develops a hematoma in the first few hours and days (Figure 2(A)). Subsequently, the inflammatory cells such macrophages, monocytes, lymphocytes and polymorphonuclear cells, and fibroblasts infiltrate the bone[18,19], that forms a granulated tissue promoting the ingrowth of vascular tissue and the migration of mesenchymal cells. The repair stage is known by the beginning of fibroblasts help for the vascular ingrowth, in order to form the bone callus. With this vascular ingrowth, there is a formation of a soft callus around the site, (Figure 2(B)). Eventually the callus ossifies, incorporating the fracture fragments (Figure 2(C)). The third stage is represented when the healing bone is restored to its original shape, structure and mechanical strength, (Figure 2(D))

[18,19]. When the fractures are severe, it is required the use of a biomaterial in order to substitute the damaged areas and stimulate the growth of bone tissue in the fracture site[20].

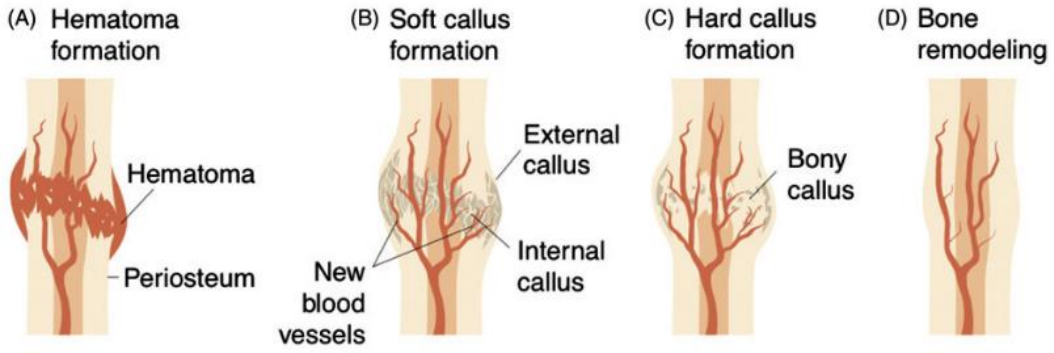

Figure 2. Different stages of bone healing.[18]

2.2. Tissue Engineering for Bone Regeneration

Bone has a known healing and regenerating process. Yet it cannot accomplish a large repair extent to regenerate large bone defects. Because of this impossibility, the development of novel biomaterials has grown through times[1]. In the past, the materials implanted were designed to be “Bio-inert”, as they were placed in the organism and substitute the damage tissue and give mechanical support with a minimal biologic response. After that, the objective was to increase the lifetime of the biomaterials inside the body by the establishment of interactions with the native tissue[21].Significant efforts have been dedicated to the development of synthetic materials to incorporate in the individual, as an alternative to create grafts to restore the form and function of the injured bone. These materials are usually designated as third generation biomaterials and must have some specific properties in order to result in a better outcome, when incorporated in human body[1]. For bone, the main goal of the biomaterials is to appropriately mimic the structure and function of the natural bone extracellular matrix (ECM)[2], in order to provide a three-dimensional (3D) environment with some specific biological characteristics that promotes the attachment, migration proliferation and differentiation of the cells[2]. Moreover, it needs to be biocompatible, avoiding an immune response and be biodegradable

with controlled degradation rate, ideally with the amount of new tissue created occurring at the same rate of biomaterial degraded[1]. They should also contain osteogenic, osteoinductive (capable of promoting the differentiation of progenitor cells down an osteoblastic lineage) and osteoconductive (support bone growth and encourage the ingrowth of surrounding bone) properties and have the necessary mechanical features in order to promote the vascularization[1]. This means that, biomaterials should possess adequate biophysical and biochemical features to induce the bone self repair[1]. Other important characteristic of the biomaterials is to be easily and efficiently reproducible in different shapes and sizes.Currently, biomaterials obtained from natural sources have become relevant options for tissue engineering applications due to their large availability and improved biological performance[22]. In this context, biomaterials from marine origin have been highlighted due to their wide range of properties and feature beneficial for their application in the medical field.

2.2.1. Marine sponges

Marine sponges are considered very relevant elements in nature because of the crucial role that they play in the equilibrium of natural ecosystems. They are among the oldest multicellular invertebrates, with little differentiation and tissue coordination, existing for around 750 million years[23,24]. Sponges do not have nervous, digestive, or circulatory systems[25], but they possess a porous structure with channels that is uniformly distributed by the full body. Their potential is revealed by the natural ability to filter seawater. The body structure of the sponges allows the flow of the water and get food and oxygen and remove wastes[25]. In fact, they can filter up to 24,000 L of seawater per kg sponge per day. Although their important ecological role in marine ecosystem it is unquestionable, they present a high potential for providing new natural products and therapeutic drugs with perspective to improve the quality of human life. These bioactive compounds result of sponges' interactions with symbiotic bacteria belonging to different phyla[26]. Consequently, they can present a high economic value as sources of biologically active compounds in pharmaceutical, cosmetic and food industry. In fact, they have more biologically active compounds than another marine organism, presenting a high commercial and pharmaceutical

value[27]. In ancient time, sponges were used in painting, hygiene, gynecology, as protective element in helmets and in medicine at cleansing and drying wounds[28]. Nowadays, they are used in fertilizers, disinfection, cosmetics, wound dressings, TE and biotechnological field regarding to their antitumor, antiviral, anti-inflammatory and antibiotic effects[26,28].

There is a large variety of sponge species. The members of Phylum Porifera are known for being multicellular, and show diversity, which results in different elasticity levels, according with cell lineages presented. These ancestral animals are usually described in four classes. The first class is Hexactinellida and these are of marine origin with siliceous sponges being largely restricted to the deep sea[27]. Homoscleromorpha is a class which represents a small group of marine sponge that is characterized by the presence of a basal membrane of collagen type IV and an aquiferous system with leuconoid organization with eurypylous, diplodal, or aphodal choanocyte chambers[24,27]. Calcarea is a class characterized by calcium carbonate spicules that are excreted to the extracellular space[27]. Demospongiae is the largest class, integrating 80% of all living sponges (Figure 3)[28].

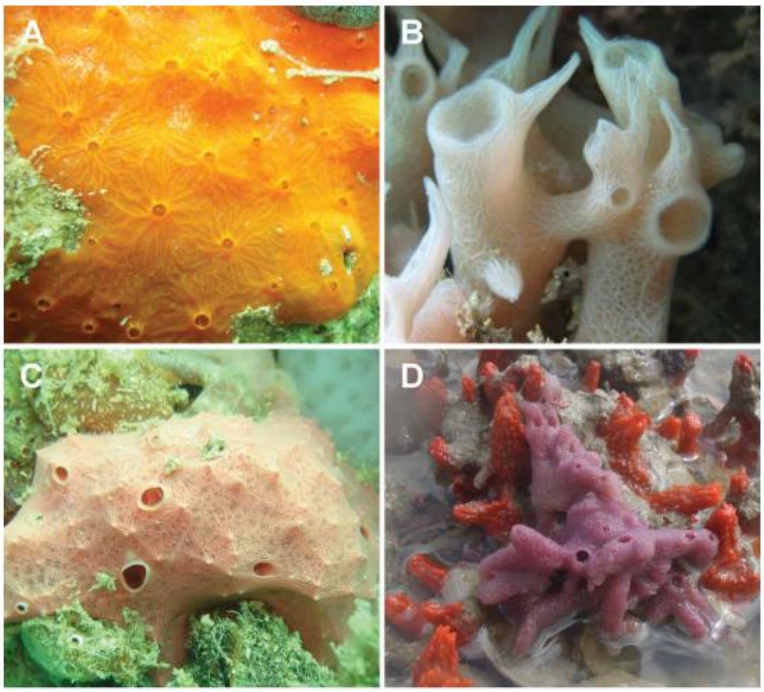

Figure 3. Examples of different demosponges (A) Clathria shoenus, (B) Haliclona sp., (C) Aplysilla aff. Rosea, (D) Haliclona implexiformis (smooth surface) and Tedania ignis (irregular).[24]

Hippospongia communis is a Demosponge, that belongs to the Dictyoceratida order and family species of Spongiidae, also known as 'honeycomb' sponge. It is one of the most abundant and has high commercial value in the world sponge market being currently mass harvested throughout the Mediterranean Sea (Figure 4A)[29]. They often grow at the entrance of underwater caves or in coralligenous formations, between 10 to 25 m depth. In shallow waters of tunisian islands, Kerkennah, these sponges are massive in shape with a diameter between 20 and 45 cm [29]. In terms of color, the surface is in tones of black/grey, and in the interior presents cream-colored to orange [29]. They are classified as hermaphroditic and in terms of life cycle, the zygote develops into parenchymella larva, being able to swim freely before settling down on a substrate where it grows into a young sponge[29].

Figure 4. Hippospongia communis geographic distribution.[30]

The body of the sponge is also crossed by wide canals, often containing large openings with a diameter of 0.06 mm to 0.1 mm and the small pores have a diameter of 0.025 to 0.03 mm. Due to this, these sponges present a firm and elastic consistency. The morphology, biologic reproduction and development of marine organisms can be influenced by the surrounding environment such as substrate, light, salinity, water motion, nutrients, and temperature. However, the temperature is generally considered to be the most important factor affecting distribution, metabolic processes, and life cycle events of these marine organisms. In Kerkennah waters, the temperature can vary between 12°C and 30°C[29].

2.2.1.1. Chemical composition

Because of the large availability of Demosponges, it became one of the class with most interest. It is composed by a single-celled epithelial layer named pinacoderm surrounding an extracellular matrix made of fibrillar collagen and reinforced by mineral spicules, spongin fiber and relates cells and skeletal components[15,25]. The inorganic elements that contribute to skeleton are an amorphous, hydrated monocrystalline silica with high water content (SiO_2/H_2O), silicon, oxygen, and small amounts of elements like Al, Ca, Cl, Cu, Fe, K, Na, S and Zn[15]. Because of its layered structure and hydrated nature, it results on an improved elasticity. It is guided by a collagen organic matrix to form a unique and

organized structure and serves as structural support. Marine sponges are the only organisms that are able to polymerize silica enzymatically and generate siliceous spicules [15,26]. These spicules can be intra or extracellular, depending on the species (Figure 5), and are produced by of specialized cells, the sclerocytes. It can be observed in a few demosponges a thin layer of soft tissues with siliceous spicules grow over a solid calcareous base[15]. With these spicules, they are regularly surrounded with an analogous collagen fiber: the spongin.

Spongin is a modified collagenous protein, being secreted by spongocytes. Its chemistry is extremely complex, due to the presence of some halogens that never been reported in natural collagens. Spongin is resistant to various enzymes such as proteases, trypsin, pronase, collagenase, amylases and lysozymes, when compared with the collagen[15,26,27]. This protein has high porosity, thermostability and form a rigid mechanical structure. The elasticity of the sponges are the result of the different ways of spongin arrangement[15,28]. Chitin is also a relevant component in sponges, being a thermostable, non-toxic, biocompatible biopolymer with good mechanical properties[26].

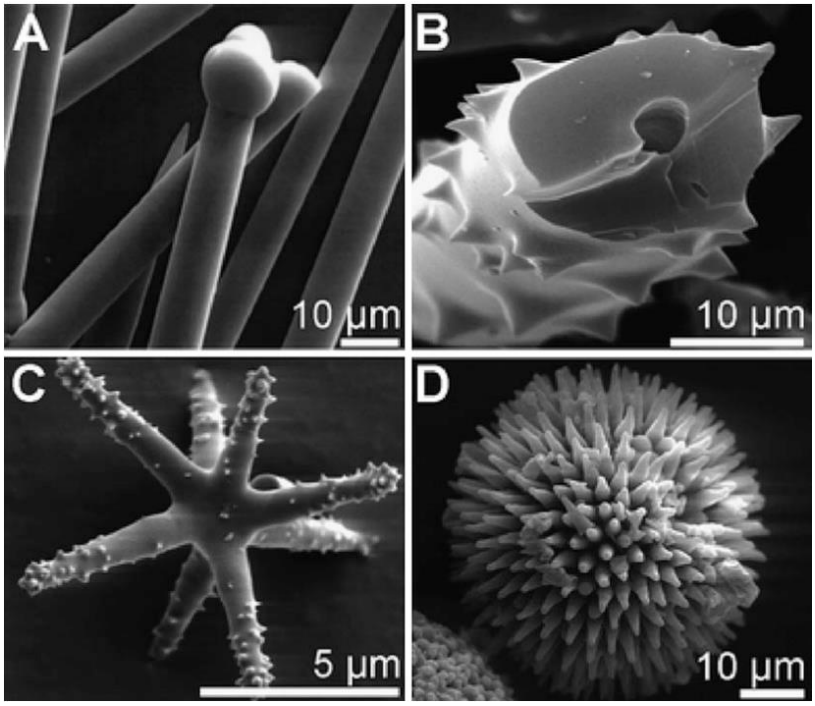

Figure 5. SEM analysis of spicules (a) (b) and spheraster (c),(d) from the marine demosponges.[31]

Other inorganic compound found in marine sponges is polyphosphate, that usually appears as tiny white clusters or granules, when sponges are observed on electron microscopy[15]. Calcium carbonate is formed by the specialized cells that filter the water and continue the biomineralization process to produce calcitic spicules[26].

2.2.1.2. Structural features

Marine sponges can be characterized by various parameters, like fineness, absorptiveness, toughness, elasticity and durability that are variable, depending of the species[28]. Usually, the sponge skeleton is characterized by a porous architecture, very organized that allows to process a great amount of water. With the increase of porosity, pore size and interconnectivity, it allows better integration of soft materials. These characteristics are very important when used as a scaffold. The compressibility and elasticity are determined by the network structure of spongin fibers (Figure 6)[28].

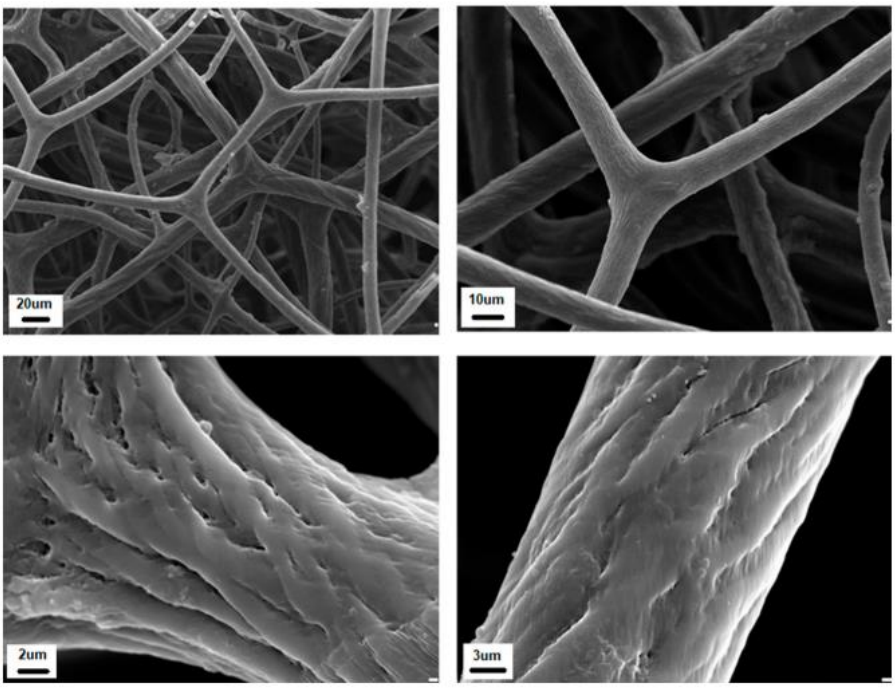

Figure 6. SEM images of *H. communis* sponge skeleton.[32]

The sponge skeleton is also constituted by silicon spicules, that plays an important role as a defence mechanism of the predators. Because of the spicules, they form a rigid framework that tends to make sponges stiff and tough, but at same time flexible[25]. The mechanical properties of the different constituents of the marine sponges are resumed at Table 2.

Table 2. Mechanical properties of selected marine biological materials.[33]

Material	Elastic modulus (E) (GPa)	Ultimate compressive strength (MPa)	Ultimate tensile strength (MPa)
Type I collagen	0.05–1GPa		20–100
Chitin	1–20		200
Calcium carbonate	50–150	100–200	
Amorphous silica	60–75	155–200	

2.2.2. Biomedical applications of marine sponge constituents

Natural marine materials are an emerging class of materials being investigated for biomedical applications. Marine sponges are constituted by several different biocomponents, where each one is characterized by providing

positive characteristics to achieve high-performance material for biomedical and bioengineering applications.

The use of collagen-based biomaterials in the field of TE applications has been intensively growing over the past decades. Collagen has applications in biomedicine, food science and cosmetics[23]. Collagen derived from marine sources can be considered as a safer alternative to bovine and porcine collagen, because of the risks of transmitting diseases [23,31]. Collagenous from marine sponges already showned to be successful templates for the formation and support of musculoskeletal tissue in vitro and in vivo[23].Its derivative, spongin, has been also showing tremendous potential to promote cell attachment, adhesion, and proliferation[24]. The most important parameter with the use in artificial bone is the mechanical strength, osteoconductivity and osteoinductivity[23]. Although these interesting properties, there are important scientific challenges to overcome for isolation and purification of marine sponge collagens.

Biossilica is also a very important biomaterial when used as scaffolds. For example, biossilica is an excellent biocompatible material with a huge potential for biomedical applications, having beneficial effect on bone and cartilage healing, inducing osteogenesis and being responsible for structural reconstruction of the biological functions[23,26,32]. It has been reported that silica is a component of many materials used as scaffold in bone and cartilage TE, including bioactive glass and composite materials.[23]

Polyphosphate can also induce differentiation of multipotent stromal cells in the different osteogenic cells. This biopolymer acts as an extracellular system for storage and delivery of energy, having an active functional role in extracellular reaction of the bone biomineralization and is promising to be used with bone biomimetic strategies[24].

2.3. Nanotechnology

Nanotechnology can be defined as an emerging area in science and engineering that involves the obtention of fundamental knowledge and their application to the design, synthesis, characterization, of materials and devices when they are confined to the nanoscale (< 100 nm)[34]. The ability to control atoms

and molecules at nanoscale allows the appearance of novel properties that can be not observed in bulk materials. With this approach, the resultant material will be improved with new characteristics. [9] The nanomaterials have found a huge potential in diverse fields of science such as chemistry, biology, materials science and engineering[9].

2.3.1. Graphene

Graphene is a nanomaterial that belongs to the family carbon allotrope, also designated as a nanocarbons, where the carbon atoms are arranged in an bidimensional hexagonal structure, looking like honey comb, with an atomic thickness[6,35]. This designation come from the “graph” for graphite and the suffix “-ene” meaning the polycondensed aromatic hydrocarbons[36]. The two-dimensional planar structure of graphene provides singular features like large surface area, high chemical and mechanical stability and outstanding thermal and electrical conductivity and transmittance (Table 3)[37].

Table 3. Graphene features.[17,38]

Specific surface area	2630 m^2g^{-1}
Charge mobility	200 000 $cm^2v^{-1}s^{-1}$
Young’s Modulus	~1.0 TPa
Thermic conductivity	~5000 $Wm^{-1}K^{-1}$
Transmittance	~97.7%

Graphene is considered a very versatile nanomaterial, being already explored in many different areas, such as electronics, biomedical technology, energy harvesting and storage, composites and coatings (Figure 7). For example, graphene can be applied as efficient and precise sensors, faster and efficient electronics, flexible displays, efficient solar panels, batteries and supercapacitors, for the development of devices able to store more energy and be faster charged[39]. This nanomaterial also presents a great potential to make heat-spreading solutions and thermal foils for mobile devices. Recently, extreme attention have

been given, healthcare applications, including drug delivery and bioimaging agents, and for the development smart scaffolds for TE applications[40].

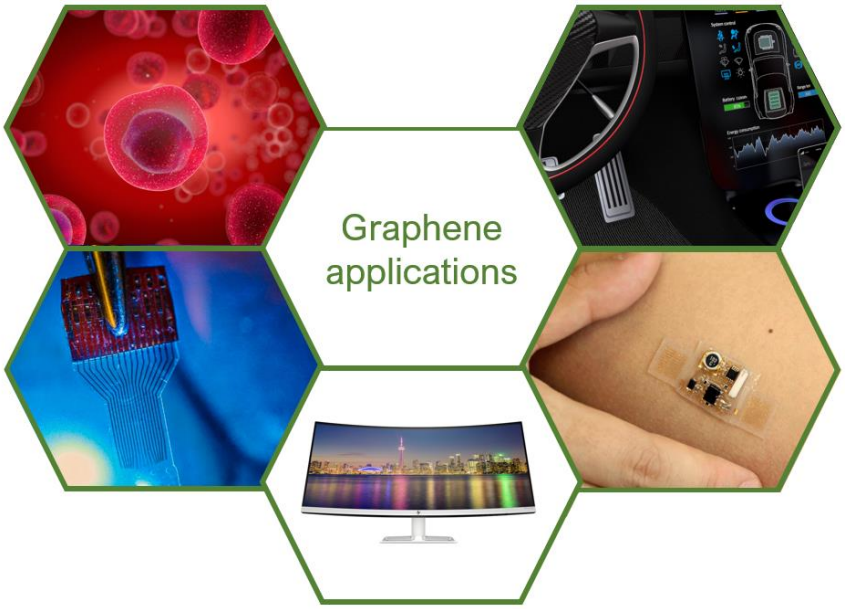

Figure 7. Graphene potential applications.

2.3.1.1. Graphene Production Techniques

The first isolated graphene sheet was produced by the mechanical exfoliation of graphite, currently designated as a scotch-tape method[41]. After that many methodologies have been developed with the purpose to produce graphene in a large scale, high quality and low-cost.

Nowadays, the different strategies to produce graphene can be divided in two main methodologies (Figure 8):

- **Top-down:** separation of an individual layer from a block of graphite layers, by overcoming the Van der Walls forces between the indiviudal carbon layers[42]. One example of this technique is the mechanical exfoliation, obtained by peeling repeatedly of a graphite block with double-sided adhesive[36]. This technique does not allow to control the number of peeled layers. Besides the resultant materials present some structural defects on carbon wire[17].

- **Bottom-up:** explores carbon molecules as building blocks, in order to form a thin layers of graphene[43]. An example of this approach is Chemical Vapour Deposition (CVD), where a solid catalytic substrate is explored for the growth of graphene, by the molecular deposition of molecular methane in gas phase. The down side is that this technique is very difficult to replicate in large scale and it presents the formation of defects on graphene grain boundaries, usually associated to the grain size and orientation of the catalytic subtract[17,43].

Other examples for the preparation of graphene nanosheets are reported at Figure 8. This schematic representation presents the advantages and disadvantages of each methodology explored according to the price and the quality of graphene flakes produced.

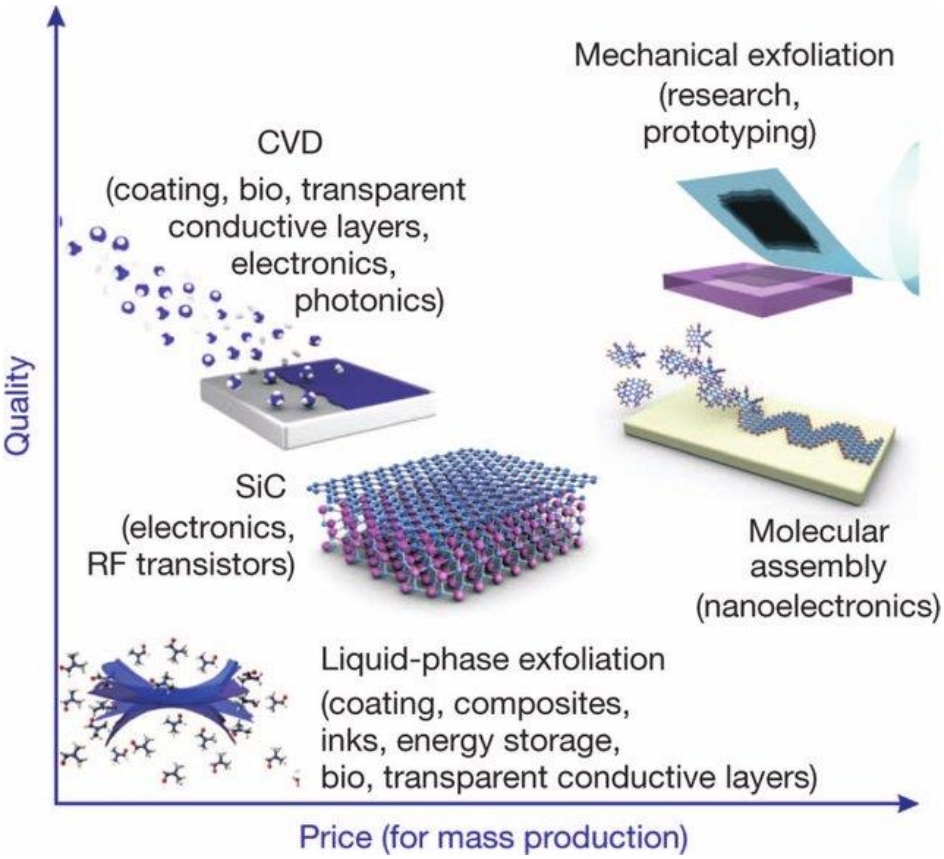

Figure 8. Schematic representation of methods for mass production of graphene. The various methods for graphene production allowing a wide choice in terms of quality and price for different applications.[44]

Looking at these two approaches, the synthesis of graphene by the bottom-up approach has proven to be the most difficult to obtain due to the requirement of advanced equipment or extensive synthetic protocols. The top-down approach is currently the most adopted approach due to the simplicity to obtain graphene and the possibility of large-scale production. However, the quality of graphene is usually significantly compromised by using this approach (Figure 8).Importantly, the graphene production method should be carefully chosen according to the final application requirements[45].

2.3.2. Graphene Oxide

Graphene oxide (GO) is an intermediate carbon-based material for the preparation of graphene. GO consists in a single atomic sheet of carbon atoms with sp^2 and sp^3 hybridized bonds. It contains oxygen functional groups like hydroxyl (–OH), alkoxy (C–O–C) in basal plans and carbonyl (C—O), carboxylic acid (–COOH) in the regions of the frontier. The presence of these reactive groups on its surface, induces high hydrophilic character to this class of nanomaterials. Besides, the presence of these functional groups provides to GO a high versatility for their surface modification by exploring a wide range of chemical routes for the covalent or non-covalent functionalization. In fact, it was observed that properties are also favorable for the adsorption of several proteins and other relevant biomolecules[6,8,36].

To synthesize GO, it must have in account characteristics like structure, size shape and functional groups desired on its surface[8]. GO can be obtained by oxidation of graphite, using oxidant reactants that influence the surface chemistry and chemo-physical properties[42]. The most used method is designated as modified Hummers' method (Figure 9), that consist on the chemical exfoliation of graphite, using a protonated solvent (like sulfuric acid, phosphoric acid) and a strong oxidizing agent like $KMnO_4$ (instead of $KClO_3$, which has toxic ClO_2 gas)[8,17,46]. After that, the purification is performed by a dilution step, and subsequently the mixture is treated with H_2O_2 to remove metal ions from the oxidizing agent. The resulting solids are separated and treated with diluted hydrochloric acid to remove any residual metal. The final step consists into wash

and centrifuge the mixture several times with water to reach a neutral pH solution. Methods like pre-treatment of graphite powders in $K_2S_2O_8$ and P_2O_5 or thermal treatment or exposure to strong oxidizers that increases the interlayer spacing resulting in an easier delamination of GO layers. Other method explored, consist on the removal of sodium nitride using phosphoric acid instead of sodium nitrate and decrease the concentration of $KMnO_4$, being this method easy to control the temperature and GO powder obtained presented a higher degree of oxidation[8].

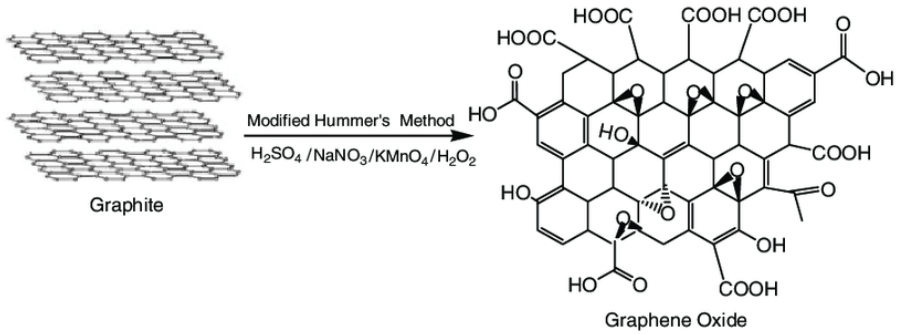

Figure 9. GO obtained by modified Hummers' method.[47]

2.3.2.1. Graphene oxide derivatives

The reduction of GO is an approach that results from additional treatments of GO in order to turn this material the closest possible to pristine Graphene. This can be achieved by removing the oxygen functional groups of GO, by exploring several chemical and physical reduction methods (Figure10). However, the final product still presents significative differences when compared to graphene, because there are difficulties in complete removal of functional groups and the reconstruction of the graphitic lattice of the material prior to the oxidation and sonication processes[42]. The reduction can be achieved in different extend according to the different methods explored[48]. The reduction of GO can be explored by using chemical or physical methods. However in order to increase the efficiency of the reduction treatment, can be explored the combination of both methodologies by the implementation of several treatment steps.[48]

The possible physical methods adopted consist in the thermal annealing at elevated temperatures in an oxygen-free environment, microwaving GO powders

or flash reduction of GO films by high-intensity light[17,43]. These techniques are extremely violent, and it can promote significant damages to carbon structure. Consequently, it can be expected that the mechanical and conductive properties decrease drastically when compared with pristine graphene[17]. The thermal reduction of GO is one of the most adopted strategies, due to its simplicity and effectiveness, and consists on the increase of temperature in an inert atmosphere, where the decomposition of oxygen functional groups into CO and CO_2 gases occurs and, consequently, gives rise to the aromatic lattice restauration [48].

Another recent technique to reduce GO is by electrochemical method where it is deposited in a substrate and it has an electron exchange between GO and electrodes of an electrochemical cell[17,43]. The use of this technique results in a material with a C/O ratio higher than compared with the chemical reduction, decreases the possibility of introducing contaminants comparing to use hydrazine and does not have secondary products of the reaction[17]. However, this methodology presents strong limitations of reproducibility when upscaled.

The reduction of GO by chemical methods is one of the most common technique implemented so far. This methodology consists of the addition of chemical reducing agents to GO solutions, like hydrazine, metal hydrides, hydrohalic acids. With the use of monohydrated hydrazine, the reactivity is smoother, being the most appealing option to reduce GO in aqueous dispersions.. Nowadays, rGO can be also synthesized with green reducing agents like ascorbic acid, sugars, amino acids and microorganisms, but it can provide some kind of contamination on the final product. After the reduction the nanomaterial tends to agglomerate and precipitate presenting large surface area, high C/O ratio and high electrical conductivity[17,43]. This method has some down sides because offers the possibility of the introduction of new doping atoms in the structure of graphene, having a strong impact on the final properties. However, these reactions can be explored for proper modulation of the electronic structure of graphene.

According to the reduction methods of GO explored, the obtained results in terms of scalability, energy usage and the amount of chemical waste is variable[43]. Furthermore, the reduction rate of GO is also significantly different. In that sense,

in some cases the reduction of GO was performed by adopting several reduction steps. For example, the use of reducing agents with chemical method have the objective of eliminate the epoxy and hydroxy groups. On the other hand, with the thermal method, it can eliminate both carboxylic and carbonyl groups. With the combination of these methods, like the use of hydrazine and thermal treatment at 100ºC, it was observed an significant improvement on the C/O ratio and conductivity of the final rGO[17].

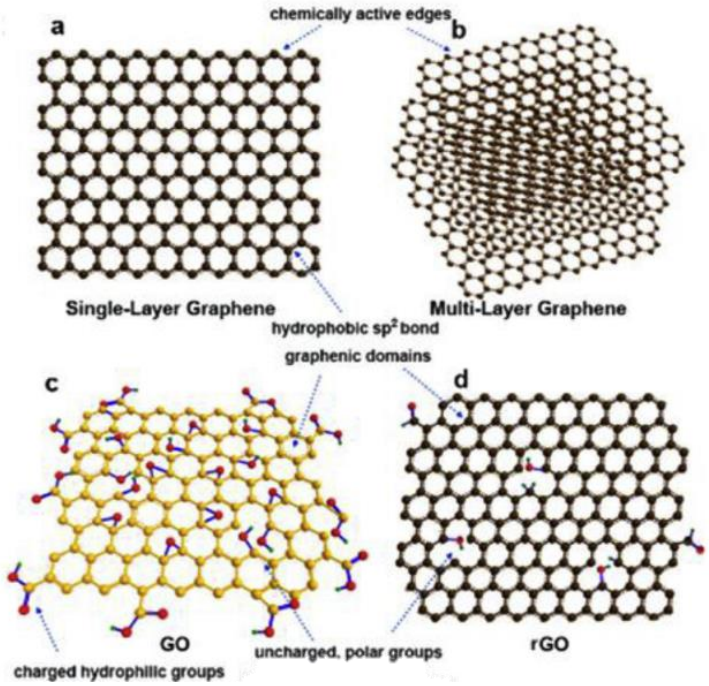

Figure 10. Graphene and its derivatives: (A) single-layer graphene, (B) multilayer graphene, (C) GO, (D) rGO.[8]

2.3.3. Graphene-based nanocomposites for biomedical applications

The term composite is used when two materials are combined in order to take advantage of their positive characteristics in a synergistic way, resulting in a material that presents an improved performance. The designation of nanocomposite material can be applied when at least one of the materials in the composite present dimensions lower than <100 nm. The main purpose of this approach is to create a combination of materials that performs better than the constituent materials alone[47]. These combinations of two or more compounds, can result in an improve of the physical and chemical proprieties of the final

product, like strength, stiffness, fatigue life, density in related to structure. There is a large sort of combinations but generally, the nanocomposite is incorporated in a matrix, that can be a polymer, ceramic or metal and a reinforcement, like nanofibers or nanoparticles.

There are several examples of this type of material in nature, being one of them the bone. Bone is composed by type I collagen fibers that are reinforced with calcium phosphate crystals, such nano hydroxyapatite[14,49].

In the recent years, graphene nanocomposites have gain a growing interest in the biomedical field The single layer carbon particle of few micrometers in lateral dimensions can directly interface with either cells or biofluids, allowing an improved performance for the development of recording, and stimulating bioelectronic devices or biosensors[50]. From the many different applications reported, it can be highlighted the application of graphene in field effect transistors for detection of biomolecules and eletrophysical signals. Because of its electrical topographical and chemical properties, graphene has a strong possibility to be explored in the biosensors field[7].

The application of GO nanosheets has some constrains resultant from their processing conditions that should be carefully addresses in the development of biomedical devices. The GO obtained from the chemical exfoliation is non homogenous and typically present a wide distribution of varying lateral dimensions and number of carbon layers, degree of functionalization and the presence of some contaminants. Despite these limitations, GO nanosheets still present some features of 2D materials, including large surface area, that combined with the surface oxygen groups that can be easily chemically functionalized, becomes an important advantage for certain biomedical applications. For these reasons, GO have been attracted considerable research interest for bioimaging and diagnostic applications, as well as vectors for drug delivery and in the development of scaffolds for tissue engineering[50]. Relevant achievements have been revealed on the development of smart scaffolds for TE[31,42]. In fact, recently it was discovered that GO not only favor stem cells attach and growth but also it increases the differentiation of those cells into specialized cells[8].I. It was also observed that by adding GO and rGO, the physiochemical and bioactivity properties of the nanocomposites suffer an improvement. This is due

to the hydrophilicity of the oxygen groups present on the surface [10]. Their polarized surface can promote the adsorption of proteins enhancing the bioactivity of the composite material. Besides, by the addition of GO, the roughness of the composite is higher, resulting at the increase of cells' spreading and osteogenic differentiation [10].

2.3.3.1. Graphene-based 3D scaffolds for smart TE

Although many researchers demonstrated the GO as a 2D scaffold with the potential to enhance cell proliferation and differentiation, it has some downsides, as 2D scaffold could not be enough, because of the topography required to have stem cell differentiation systems, as the cells do not have the channels to grow and to promote the cell-to-cell and cell-to- extracellular matrix interaction as it could happen using a 3D scaffold[7]. TE relies on the use of 3D scaffolds to provide the proper environment for the regeneration of tissues and organs. It acts like a template for tissue formation and are typically seeded with cells and sometimes with growth factors or put under biophysical stimuli to accelerate the biological process [49]. As commented above, graphene has proved to be a good material in order to induce differentiation on stem cells, when it is stimulated, giving a new path to explore. With electrical stimulation cell differentiation can be guided by a non-invasive method, using GO, in order to use in neurological diseases[7,51,52]. Pulsed laser stimulation has been used instead of electrical stimulation because it stimulates the desired tissue without having direct contact with cells and offers an improved spatial resolution of stimulation.

After observation of the mechanisms of the cell environment, it was discovered that physical and mechanical factors are fundamental in the modulation of the cell's behavior. As cells can sense forces and turn them to biochemical signals, when a mechanical stimulation is applied on its surface, the transduction occurs, and all sorts of molecules are activated[7]. Studies shown that the application of a short-term mechanical stimulation enhanced the activation of osteogenic differentiation pathways in human mesenchymal stem cells[53]. Some articles reported that graphene films and scaffolds have demonstrated osteogenic potential, as the mechanical-stimulation on cells that creates a signal transduced that results in cell responses to the environment, like proliferation, differentiation and apoptosis[54].

GO was also explored as a reinforcing agent of many natural polymers that present a high biological performance in a synergistic way. Studies demonstrated that chitosan is a natural polymer extracted from marine microorganisms, being biocompatible, biodegradable, and favorable to bone defects repair. Still, this material has poor mechanical properties and low bioactivity. With addition of GO, these inferior properties can be significantly improved [11]. This composite showed that mechanical properties like modulus of elasticity and hardness were improved and the attachment and proliferation of pre-osteoblasts were higher, representing a better biocompability and bioactivity [11]. Besides GO can contribute for the development of smart scaffolds able to induce biophysical stimulation. Recent studies have shown that graphene-based materials, specially GO, under mechanical stimulation can induce osteoblast differentiation of mesenchymal stem cells, responsible for the osteogenesis and enhancement of bone formation. With their chemicophysical properties, graphene materials family can be selected for exerting distinct molecular effects on the immune cells that improves new immune-based strategies in osteogenesis and bone regeneration[7,55].

2.3.3.2. Layer-by-layer self-assembly of graphene nanocomposites for biomedical applications

Layer-by-layer (LbL) assembly is considered one of the most promising approach for the controlled fabrication of single or multilayer thin films[26,55].These films have been created by alternating coatings of oppositely charged solubilized polymers, forming polyelectrolyte multilayers. This technique explores the combination of oppositely-charged polyelectrolytes, can be easily adapted and modified for the developmentin a wide variety of functional materials (Figure 11) [10,13,56,57] The composition, thickness and architecture of these coatings can be controlled in the nano- or micro- scale[58]. Some of the positive polyeletrolyte, such as chitosan, polyamide, poly(diallyldimethylammonium chloride) (PDDA) and polyethyleneimine (PEI) were used in order to promote the establishment of stable electrostatic interactions[10,13]. The use of this technique can promote enhancement of different phenomena such as transport properties, hydrophilicity, and contamination resistance[10]. Carbon-based nanomaterials are very versatile in terms of chemical structure, which makes it easy to host and grow different

architectures of multifunctional coatings by LbL on the surface of several matrices[59].

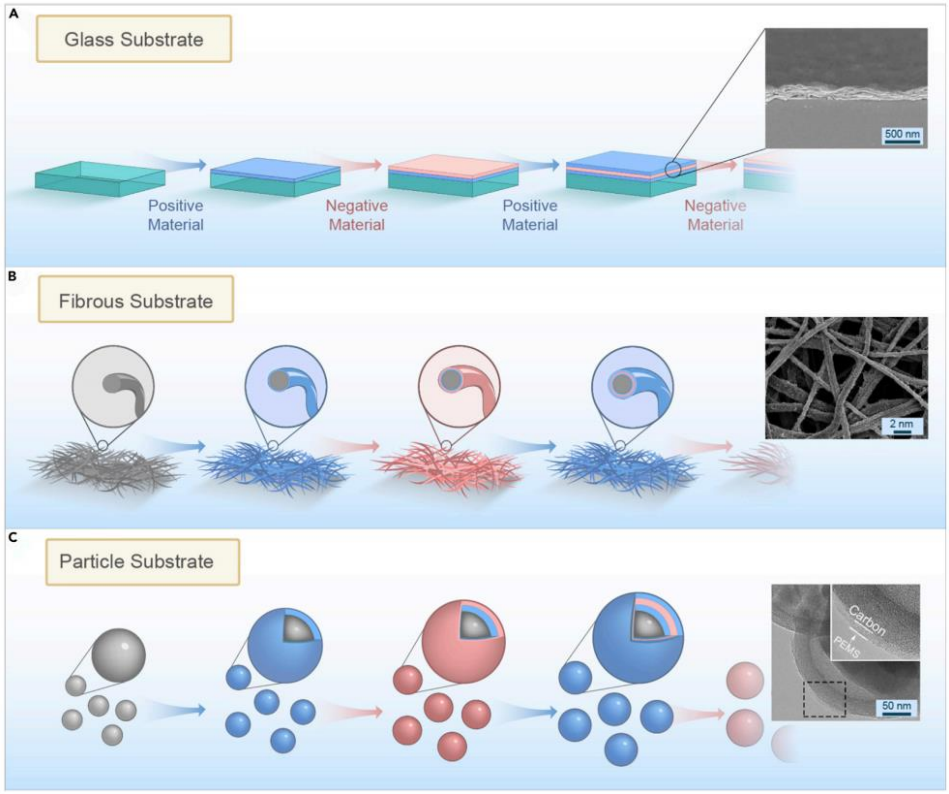

Figure 11. Layer-by-Layer assembly based on electrostatic interactions used in different substrates.[57]

Recently, this method benefited areas related to nanoscience and nanotechnology. Because of the use of oppositely charged materials, the resulted material is built up a multilayered architecture via electrostatic interactions to form highly stable nanostructured films on a solid substrate. This method has proved to be attractive to study new sensors and biosensors systems, as the film acts as a biocompatible layer into the sensing unit representing the sensor surface and it is responsible for the molecular recognition between the device and the substance to be detected[60]. This alternation of the surface charge allows the binding with biological substances, such proteins, nucleic acids, organic polymers and inorganic substances. With the high flexibility yet structurally resilient films resulted from the LbL method, a variety of biomaterials can be integrated into custom-made layer structures[61]. Consequently, their practical use as drug carriers for controlled delivery have been developed of LbL microcapsules pores composed of polyelectrolytes by changing the surrounding solvents[61]. GO

membranes can be prepared with LBL self-assembly, as it provides integrity for the membrane giving it better stability[62]. Moreover, LBL assembly of GO nanosheets with alternate fibrinogen nanofibers were also explored for the surface modification of silicon substrate in order to fabricated 3D scaffolds, able to provide subsequent biomimetic mineralization of hydroxyapatite (HA)[63]. The in vitro cell culture with L-929 fibroblasts showed that GO-based scaffold improved biocompatibility and the cell proliferation.

As the adsorption of these cells are critical for the properties of the surface of the scaffold, such as wettability, roughness, surface charge, and chemical functionality, the modification of this material can give in different[64]. The reduction of GO sheets in LbL film is generally performed by thermal treatment, chemical reduction, and electrochemical reaction to restore the unique properties of graphene, while keeping the properties of polymer counterparts intact. Graphene-polymer nanocomposites have been widely studied for high performance materials because of the graphene's mechanical properties[57,65] and ability to induce cell behaviour. Recently, it was reported that partially reduced GO (rGO) nanosheets combined with polycaprolactone–gelatin electrospun nanofibrous are able to form 3D-rGO heterogeneous porous networks suitable for enhancing adhesion and differentiation of neural cells[66].

CHAPTER 3

3. Synthesis and characterization of MS/GO nanocomposites by LbL

3.1. Materials and methods

3.1.1. Purification of spongin skeleton

Sponges skeleton (MS) were purchased from Nuvaria Global. The sponges were first cut into cubes with dimension of ~125 mm^3. The samples were purified by washing them with ultrapure water (water distillation system from Wasserlab®), to remove residual salts[67]. Then, it was applied an hydrochloric acid solution (HCl) 0.5 M to remove the residual calcium carbonate microparticles and silica spicules [67]. After that, the samples were rinsed in distilled water to remove the residues of HCl. Some samples went through a thermal treatment with the increase of temperature to 180 °C in a vacuum oven (Thermo scientific).

3.1.2. Synthesis of MS/GO scaffolds by LbL

To synthesize the novel nanocomposite materials, MS surface was modified by LbL using different polyelectrolytes. The positively charged polyelectrolytes Polyethylenimine (PEI, with a Mw~800 by LS, average Mn~600 by GPC) and poly(diallyldimethylammonium chloride (PDDA with low molecular weight, 20 wt.% in water) from the Sigma Aldrich®, were used as an intermediate layer for producing the scaffolds. The negatively charged GO was used in water dispersion (4mg/mL of Graphenea SA) for the functionalization of MS surface.

3.1.3. Characterization of MS nanocomposites

The structural analysis of MS and new derivates was firstly analyzed by Scanning Electron Microscopy (SEM) with Philips XL 30 ESEMFEM These samples were prepared with carbon glue between them and the platform with amplifications of x300 and x3k. The samples were analyzed to find out the density

of this material, so it was studied the dimension of the fibers, with a micro-computed tomography (μCT) equipment from SkyScan 1275 (Bruker microCT, Belgium). The thermal stability was conducted by thermogravimetric analysis (TGA) (Netzsch STA 449F3). The chemical analysis was accessed by Fourier-Transform Infrared Spectroscopy (FTIR) (Bruker ALPHA FT-IR Spectrometer) recorded between 400 and 4000 cm^{-1} with a resolution of 2 cm^{-1}. The mechanical characterization of the MS and MS nanocomposites was performed by dynamic and static mechanical compression tests (Shimadzu MMT-101N). Static compression had a load cell of 100 N. The cubic shaped samples were compressed at a rate of 5 $mm.min^{-1}$ up to the maximum limit. Dynamic compressions tests were performed with a 10% of the deformation and 0.5Hz frequency of compressions for 10 000 cycles to access the mechanical stability of the sample. These tests were performed under dry and wet environment. These results will be critical to estimate the behavior of these samples under dynamic mechanical stimulation in the bioreactor.

3.1.4 Purification of GO

The commercial GO acquired from Graphenea was purified to remove potential toxic elements (resultant from the raw materials used to prepare the GO) and increase the pH of the solution to neutral. This pre-treatment is extremely important having into account that materials will be explored for biomedical applications. The initial concentration of GO was 4 mg/mL. The GO purification was conducted by performing several centrifugation cycles at 12.000 rpm for 15 minutes, having a reasonable deposition of GO. The supernatant of the suspension was removed and replaced by the same volume of distilled water (Figure 12). This process was repeated until the pH reach neutral (pH~7). In average, this procedure was performed by five times. The obtained GO is already well characterized on the previous articles published in the research group.[68]

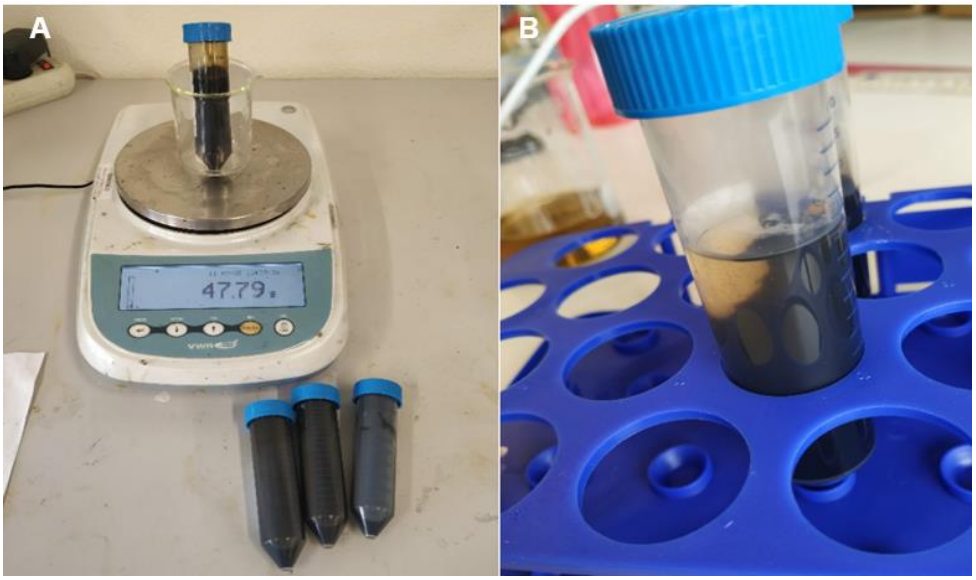

Figure 12. Purification of the GO using ultrapure water, before A) and after separation by centrifugation B).

3.2. Preparation of MS substrate

3.2.1. Chemical and structural analysis of as-received MS

In order to obtain scaffolds with similar dimensions to obtain samples as similar possible, the original MS was cut into small fractions to obtain a dense cube shaped sponge of 125mm^3 as shown in the Figure 13.

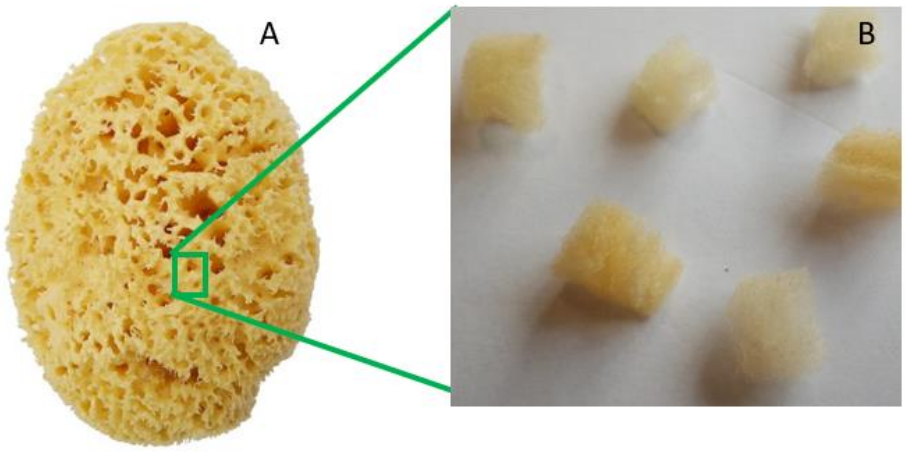

Figure 13. Image of the Original H. communis. The inset shows the cut cubes of MS with 5x5x5mm.

The structural analysis of the MS was firstly accessed by SEM (Figure 14). These SEM images shown that MS has a structure with interconnected 3D network of fibers, known by spongin[29,69]. The presence of the salt can be mainly attributed to the high concentration of salts on the ocean that penetrate the sponge and, when it dried, precipitate on their surface.

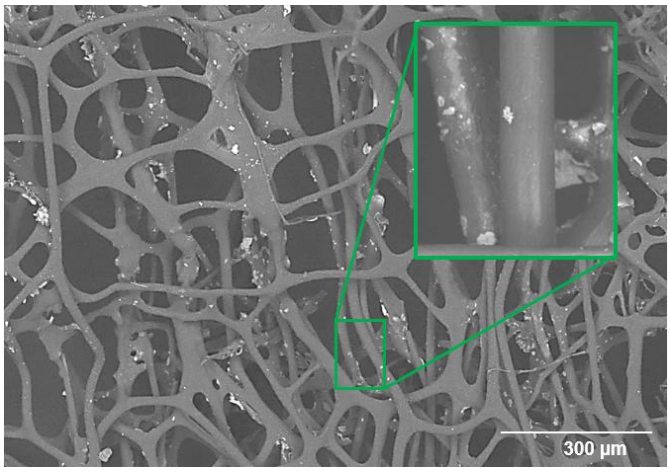

Figure 14. SEM image of the sponge as received (MS).

When analyzed using the EDS system (Figure 15), it was observed the presence of elements like Si related to monocrystalline silica usually named spicules, present on its composition and Ca, related to the base where these spicules grow over[15]. These results prove the importance to purify these sponges before their use to prepare the scaffolds.

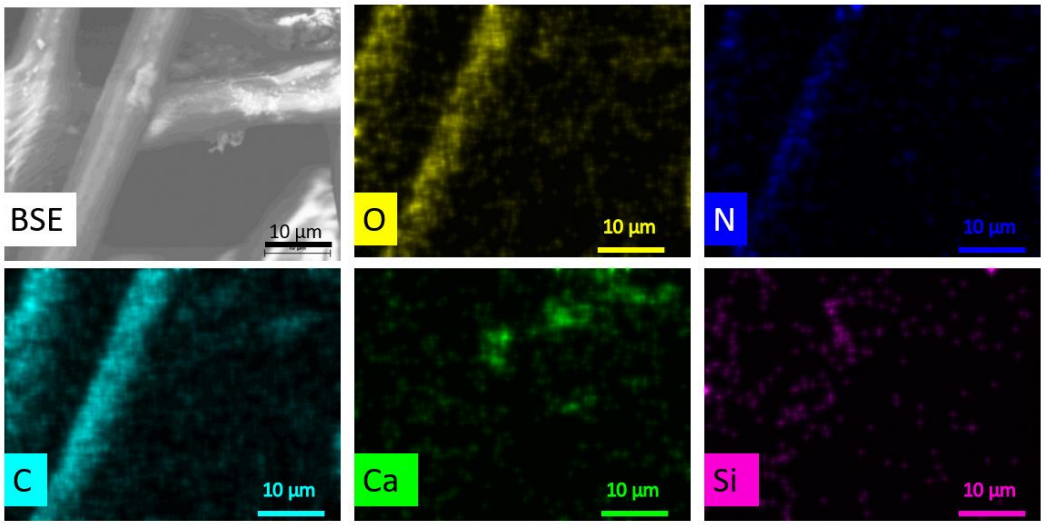

Figure 15. EDS analysis of the sponge skeleton as received (MS).

3.2.2. Purification of the MS

For the purification of MS samples, two different strategies were applied (Figure 16). In the first approach the samples were simply washed out in a water with magnetic stirring for 24 h (MSH2O). In the second approach, they were put through acid treatment under mild conditions[70]. For that purpose, a solution of

HCl was added with a concentration of 1% V/V and the sponges were dipped and stirred for about 24h (MSHCl). Then, sponges were rinsed with distilled water until neutral pH (~7) was reached to eliminate residues of HCl. With both these treatment it is expected to remove the natural impurities in form of calcium carbonate and silicates [69,71]. After purification, the scaffolds were dried at 37ºC for 24h and stored in plastic bags at room temperature.

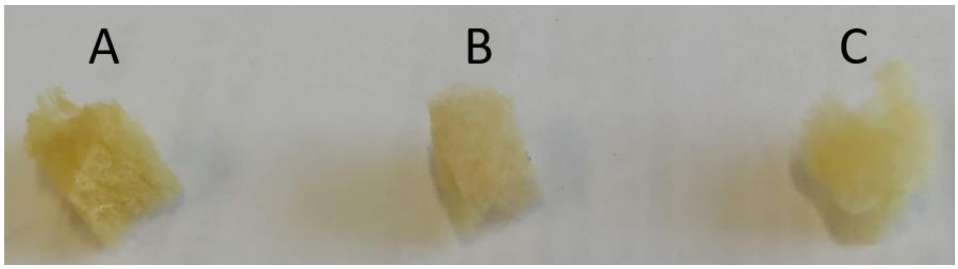

Figure 16. Sponge with any treatment (A), sponge washed with water (B) and with acid treatment (C).

The direct comparison of the samples not washed and washed by the two mentioned approaches (Figure 17), clearly show a significantly decrease of the particles on the branched structures, particularly in the sample treated with HCl, where almost no contaminations were observed on the spongin skeleton (Figure 17C).

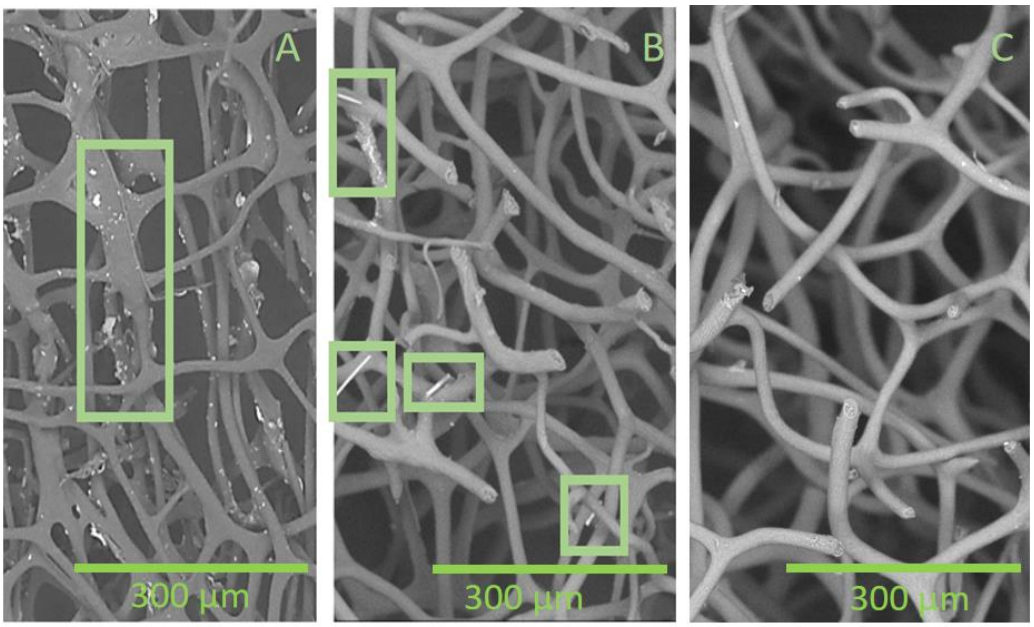

Figure 17. SEM image of MS without treatment (A), and after MSH2O (B) and MSHCl (C) treatment.

The EDS analysis of the samples treated with water presented a complete elimination of Ca elements, however it still be possible to observe the presence of Si spicules (Figure 18).

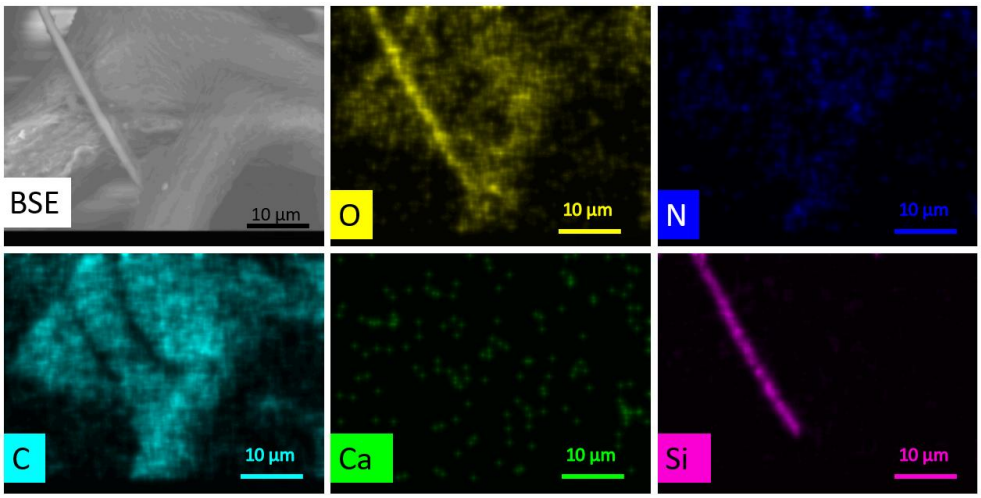

Figure 18. EDS image (BSE) and mapping of O, N, C, Ca and Si of a sample washed with ultrapure water.

The EDS analysis of the samples treated with HCl presented a structure mainly composed by O, N and C (Figure 19), without the significative presence of contaminants such as Si structures, as observed to the samples just washed with water.

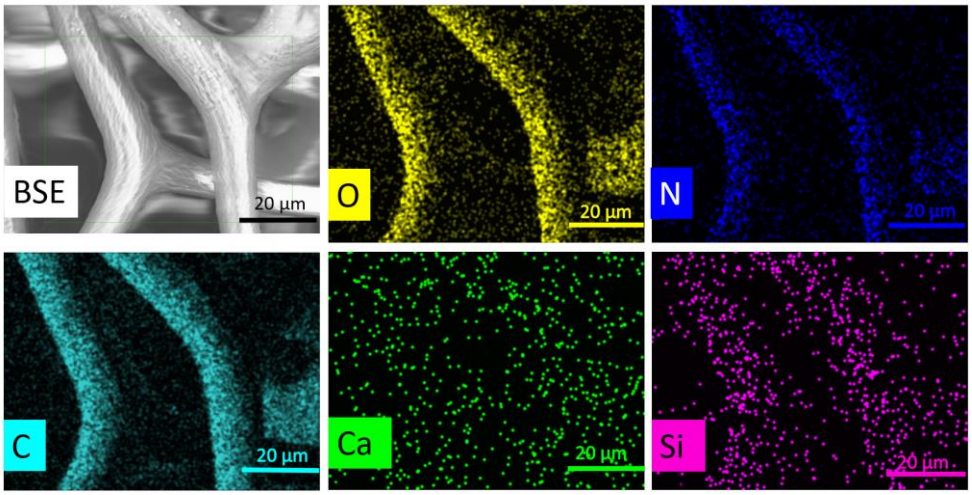

Figure 19. EDS mapping images of a sample washed with HCl.

3.2.3. Characterization of the sponge

In order to further investigate the presence of contaminants in the MS, they were analyzed by thermogravimetric analysis (TGA) in an oxygen atmosphere. The organic part of the sponge was fully degraded, resulting only the inorganic residues of the sample, which represents the portion of elements like calcium, silica and polyphosphate. The TGA analysis shows that the sponges have three discrete characteristic decomposition steps (Figure 20). The first weight loss, of about 8%, at 140 ºC can simply be ascribed to the escape of water evaporation from the sample[72]. The second step revealed a decrease of 36% of the weight when the temperature reached the 360 ºC. This decrease is related to the destruction of protein structure of the sponge skeleton[72]. The third step represents the decomposition of the organic matter of the sample, with compounds like spongin, chitin and calcium carbonate. By comparison of the different samples, the as-received sponges present highest quantity of inorganic residues (6.6%). When washed with water, the amount of residues decreases (5.9%). As the sponges were washed with the HCl treatment, the initial portion of inorganic matter was already lower than the other samples and with that, resulted in a lower inorganic content after the heating, of 3.15%. These results revealed that the samples treated with HCl presents a higher level of purification.

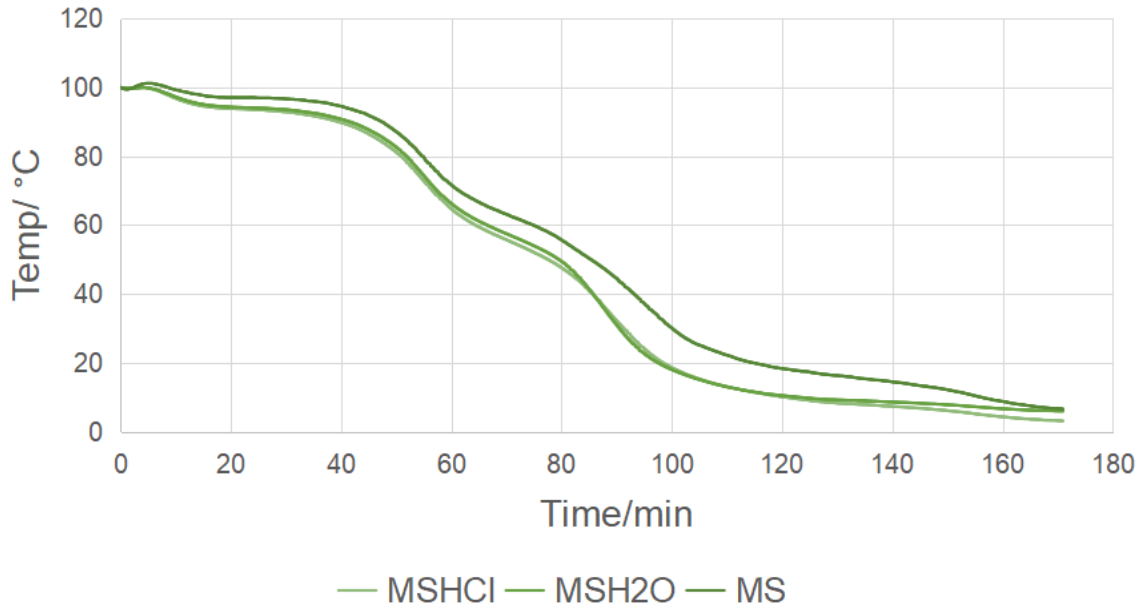

Figure 20. TGA graphic of the sponge samples under oxygen atmosphere.

3.2.4. Chemical analysis

The different MS samples were analyzed by FTIR technique (Figure 21). With this analysis, it is intended to identify the presence of organic and some inorganic materials by the presence of specific chemical bonds. Moreover, will be also possible to observe if this purification with HCl will promote structural degradation of the organic structure of MS.

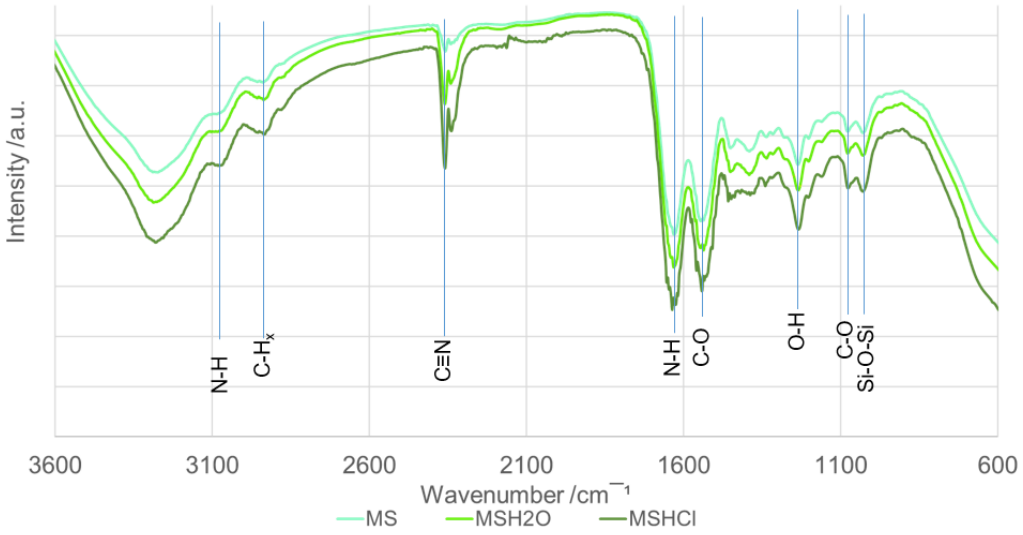

Figure 21. FTIR of the MS with different purification methods.

The FTIR analysis reveal the presence of peaks at 1021 cm^{-1} that is usually assigned to the Si-O-Si bending[73], at 1058 cm^{-1} standing for C-O bonding, that verifies the O-H group, at 1233 cm^{-1} related to amide III. That results from phase combination of C–N stretching and N–H plane bending vibrations contributing to the footprint of peptide bonds (–CONH–) that is significantly reduced in the spectrum recorded for the organic–inorganic material[72]. Peaks like 1534 cm^{-1} and 1613 cm^{-1} represents the CO and N–H stretching of amide I[72], 2359 cm^{-1} representing the C≡N stretch and 2935 cm^{-1} are related to CH_3 and CH_2 symmetric and asymmetric vibrations[74], 3070 cm^{-1} and 3278 cm^{-1} representing the N-H stretching[74]. These peaks that represent amide are related to the proteins like collagen analogous, such as the spongin. All the samples showed theses peaks, meaning that their organic phase is similar, even for MSHCl that suffered an acid treatment, showing that this method is not harmful for its structure.

3.2.5. Mechanical characterization of MS

The treated MS sponges with the different mentioned approaches were tested through compression static tests, to achieve information about their mechanical properties (Figure 22).

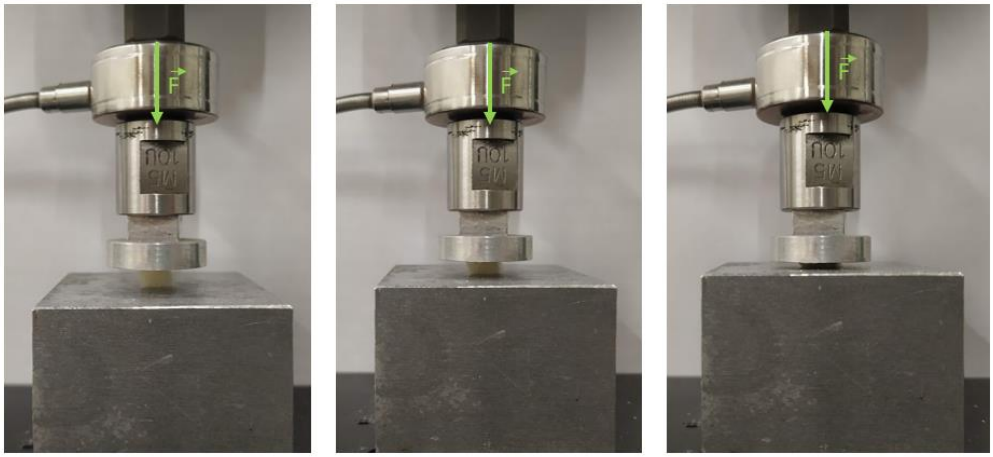

Figure 22. Static compression tests of the MS.

Although the sponges were cut into similar cubes, the results are variable for each portion because of its different porosity and density. In Figure 23, the different treated sponges presented in a similar σ-ε curve, showing a “J shape”, when they were submitted to the compression test. The sponges were compressed in totality of their form. After the test, all of them were able to recover to their original form. This indicates that the original structure of the MS was not affected during the washing protocol and the main factor for its behavior is dominated by the spongin skeleton[75].

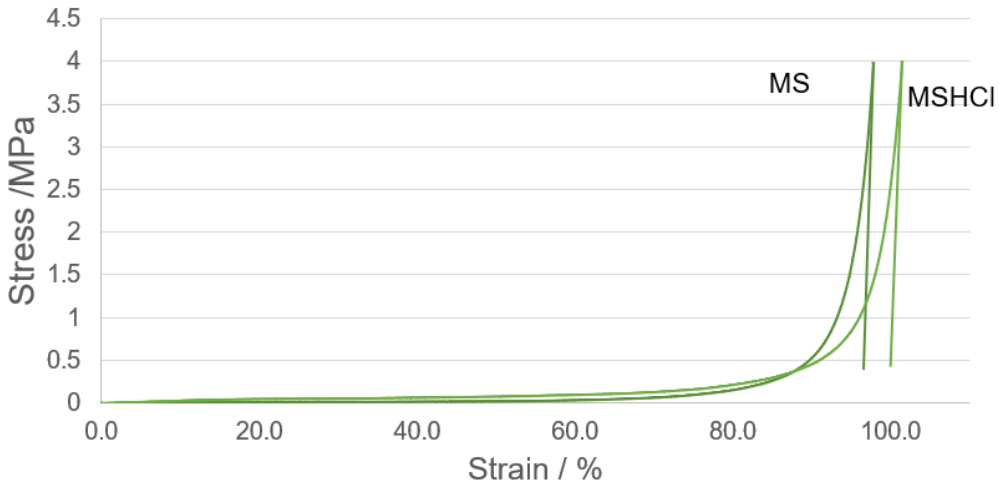

Figure 23. Strain-Stress curves of the MS and MSHCl.

As seen in Figure 23, all the sponges present the same value for the maximum stress resistance of (4 MPa). The Young modulus of the samples were calculated by the analysis of the stress – strain curves, specifically, from the slope

at low strain (0 - 10%). %). From these analyses the Young modulus of the samples was determined for the different treatments (Figure 24).

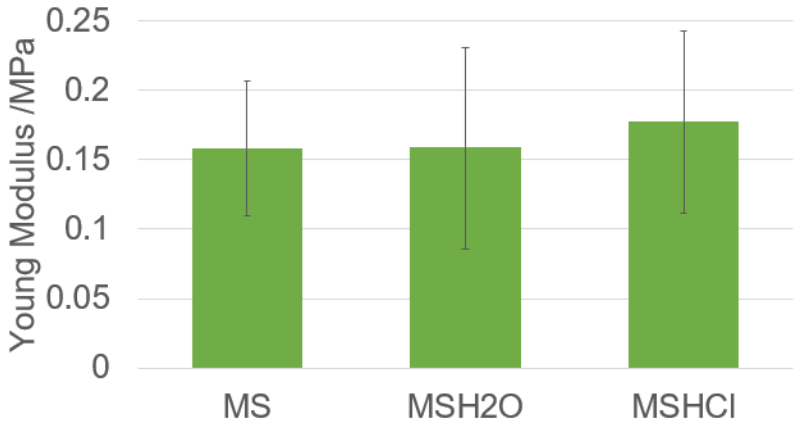

Figure 24. Young's modulus from the different purified sponges.

The MS presented a Young's modulus of 0.158±0.048 MPa, the MSH2O presented a value of 0.158±0.076MPa and with the acid treatment a slight increase to 0.177±0.066 MPa. However, these results are mainly dependent of the sample's matrix than of the treatment used. With the similar statistic values of these three samples, it can be concluded that the removal of impurities did not damaged the spongin.

The obtained values showed that the different approaches used to remove the impurities of the MS surface, did not affect their mechanical performance since they presented a similar value for the elastic modulus. Since the sample MSHCl presents the low contents of inorganic residuals and their mechanical stability was not compromised, this sample was further explored for the dynamic compression tests.

Then MSHCl samples were tested with dynamic compressions for about five hours, with a 10% of the deformation and 0.5Hz frequency of compressions for 10 000 cycles to obtain information about the stability of the sample (Figure 25).

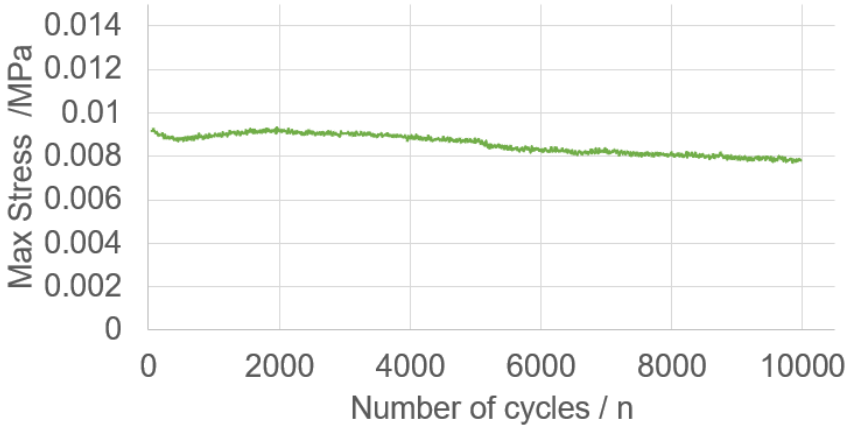

Figure 25. Dynamic test of the MSHCl sponge under 10 % of deformation.

Throughout the tests, the sample MSHCl showed a constant behavior with a maximum stress of 0.009 MPa, having about 10% of decrease in stress. At the beginning of the test, it was observed a slight adjustment of the sample that corresponds to a small decrease of its height, however after about 6000 cycles, it tends to stabilize its dimension.

3.2.6. Thermal treatment MS

After the purification of the MS by HCl, the samples were heat treated at 180 ºC during 12 h (MSTT) samples. The resultant samples were characterized to further investigate how the thermal treatment can affect their structural properties. These results are crucial in order to apply the thermal reduction protocol to MS/GBM nanocomposites.

CT scan analysis shows that the heat-treated samples showed a densification of its structure. In fact, it is observed that the average diameter of the MS fibers significantly increases due to the thermal treatment applied (Figure 26C).

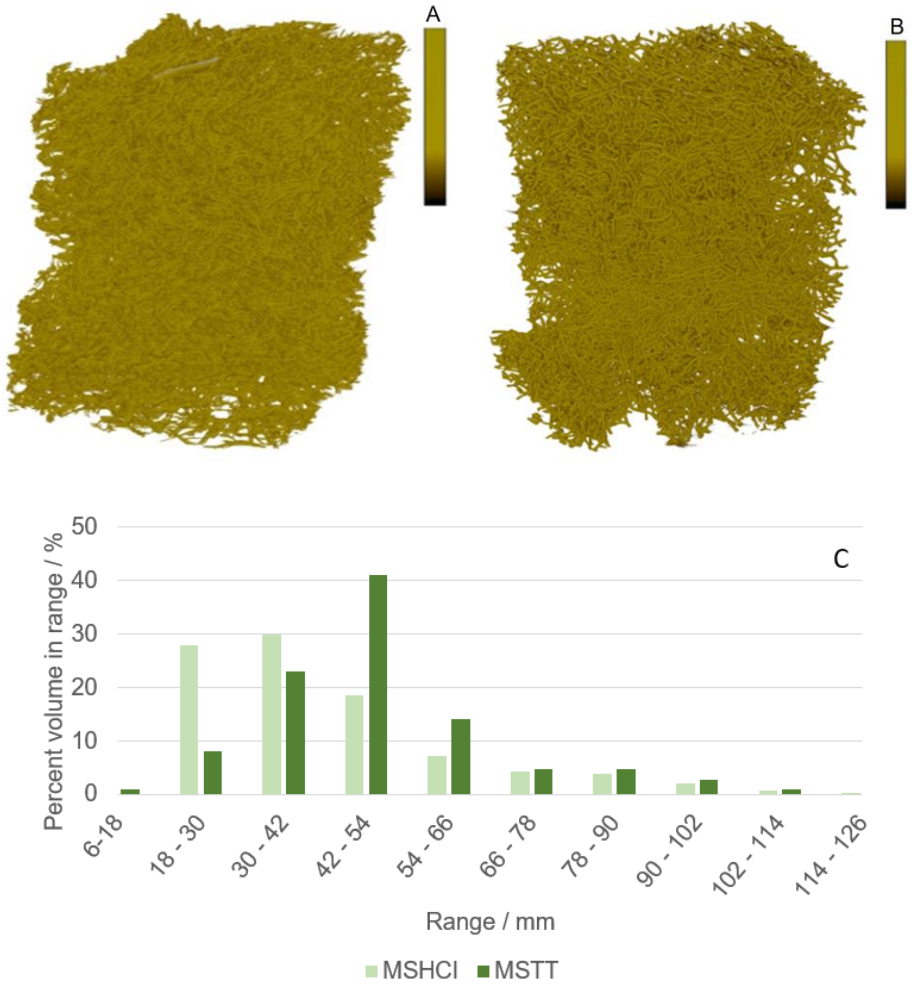

Figure 26. 3D image of the MSHCl (A) and MSTT (B) obtained by micro-CT. Comparative analysis of the diameter distribution of the MS fibers (C).

Figure 26 depicts the percentage of volume distribution of MS specimens before and after thermal treatment. The results point to an increase of the thickness of the MS fibers from 18-42 µm to the range of 42-54 µm.

With the temperature, the proteins were condensed wider, when compared with the non-treated samples. This size difference can be also observed by the SEM images from the two sponges (Figure 27). It is also observed that the surface of the fibers thermal treated are smooth and the non-thermal treated present a high rugosity.

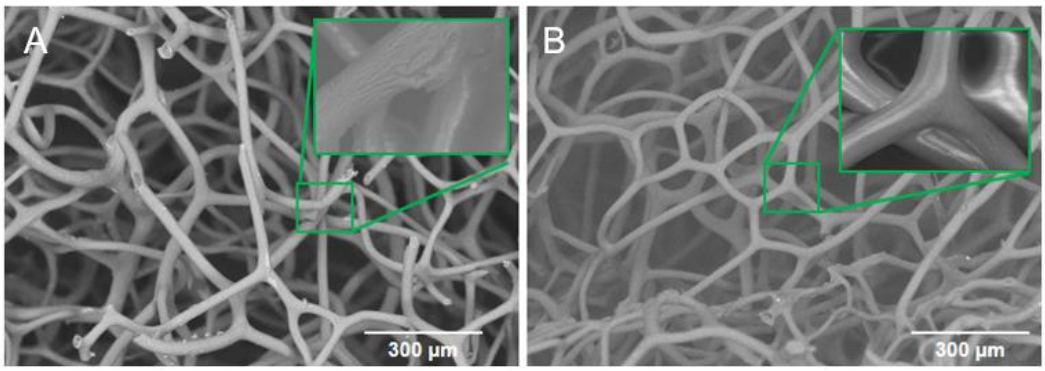

Figure 27. SEM images of MSHCl (A) and MSTT (B).

Due to the change of MSTT morphology, where the sponge tends to be denser, it was needed to investigate the mechanical properties of this material after thermal treatment. In this sense, the MSTT samples was further characterized by compression tests. When applied the compression force, the stress showed a decrease from about 4 MPa to about 0.05 MPa. The strain-stress curves showed that, the MSHCl presented a more elastic behavior for 36.8% of the strain applied, comparing with a elastic behavior of 59.72% for MSTT sample, (Figure 28). When sponges are treated with temperature, the graphic tends to present a different shape from the compression tests, that represents a plastic behavior more evident, compared with non-treated MS. Those tests resulted in a linear line, reflecting the loss of flexible properties.

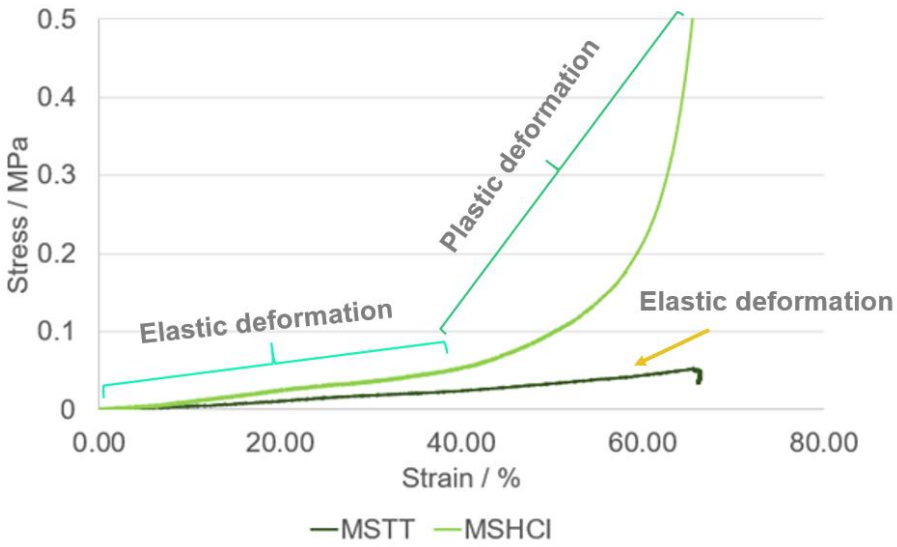

Figure 28. Strain-Stress curves of MSHCl and MSTT.

The Young modulus of the MS before and after thermal treatment was calculated and presented in the Figure 29.

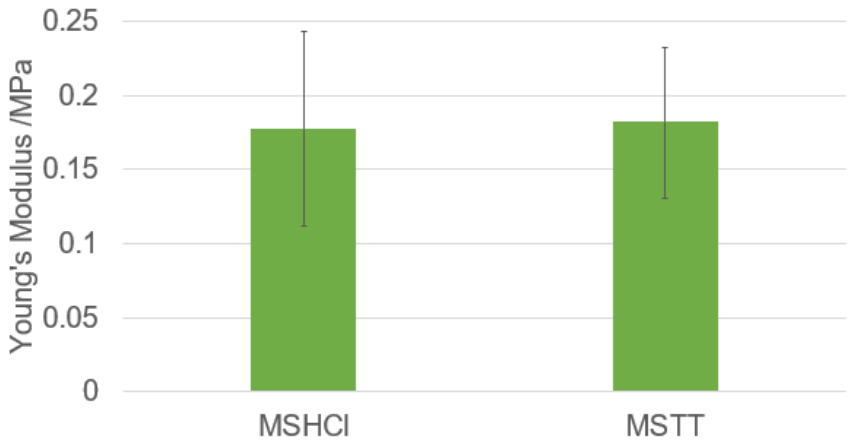

Figure 29. Young Modulus of the MSHCl and MSTT. Each value was calculated by the measurement of 5 specimens.

Because of the denaturation of proteins with the increase of temperature, sponges may tend to lose their flexibility and the capacity of recovering its form resulting on the increase of the Young's modulus. However, it was observed that although the significant morphological differences, the samples present similar values of young modulus MSHCl (0.177±0.066 MPa) and the MSTT (0.182±0.051 MPa).

When submitted to dynamic tests, the samples present a permanent shape changes in the beginning of the cycles, because of the plasticity presented by them. After 4000 cycles, the sponge tends to be more stable with number of cycles (Figure 30).

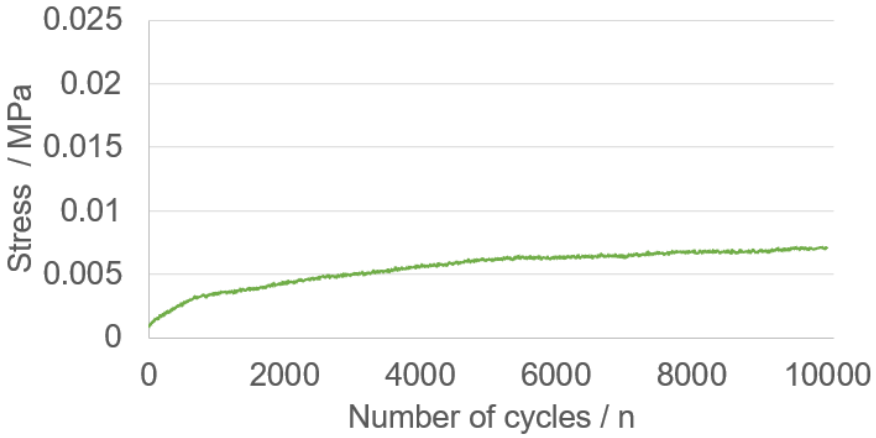

Figure 30. Dynamic test of MSTT under 10 000 cycles of compression.

The chemical composition of MSTT sample was assessed by FTIR analysis for comparison with non-treated MSHCl (Figure 31). The obtained results showed similar spectra for both samples, reflecting that the structure of the constituents of the sponge and chemical characteristics are thermically stable at 180 ºC and were not significantly damaged[76]. These results were expected, since the TGA analysis allowed to predict that at 180 ºC no significant damages of peptide structure of MS was observed[76].

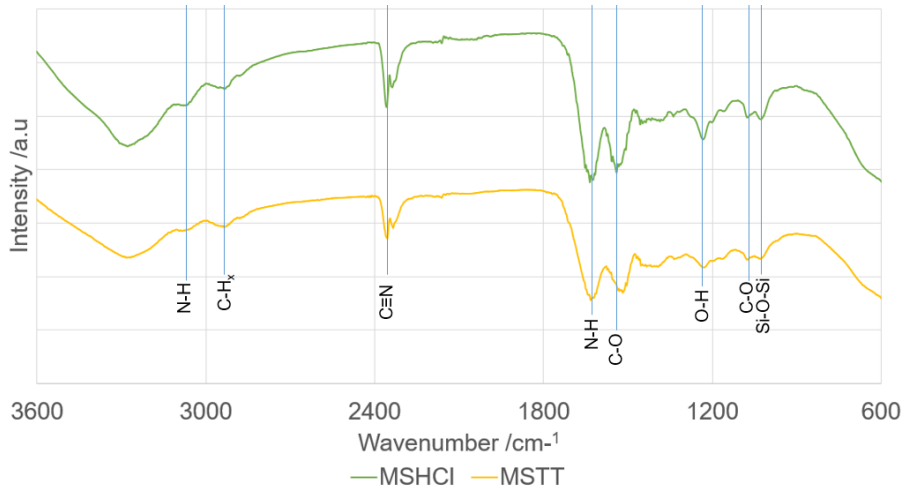

Figure 31. FTIR analysis of the sample MSHCl and MSTT.

3.3. Synthesis of MS/GO scaffolds by LbL

To modify the surface of the MS with GO, the methodology used was the LbL technique, that is considered one of the most promising approach for the controlled fabrication of single or multilayer thin films. The composition, thickness and architecture of these coatings can be precisely controlled using the combination of oppositely-charged polyeletrolytes [12,13]. As both MS and GBM are negatively charged in their surface, a interlayer of a positive polyeletrolyte, such as poly(diallyldimethylammonium chloride) (PDDA) or polyethyleneimine (PEI) was explored in order to promote a stable electrostatic interactions and with that, create a cohesive coverage as schematized in Figure 32[12,13].

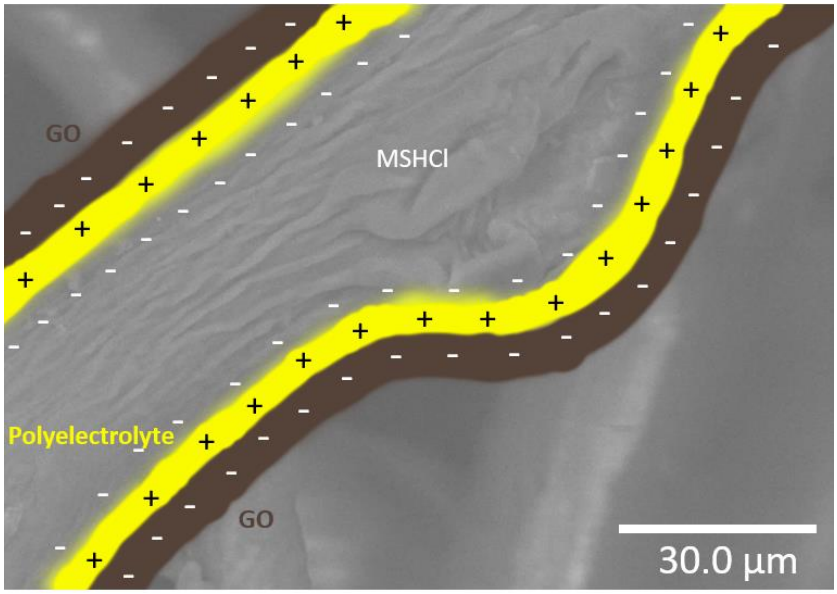

Figure 32. Scheme of the MSHCl modified with one the deposition of one layer of Polyelectrolyte/GO.

3.3.1. LbL assembly of GO on MS using polyethyleneimine (PEI)

PEI is an organic polyamine polymer and one of the most prominent examples of cationic polyelectrolyte[58,77].The amount of 2.25 g of PEI solution was diluted in 250 mL of distilled water to obtain a solution with concentration of 0.5 mg/mL. Then the obtained solution was conserved in the fridge.

The sponge samples were submersed in 15 mL of PEI solution, being removed all the air inside, and stirred for 1 hour. Then, the sponges were placed in 300 mL of distilled water and stirred for 30 minutes to remove the excess of PEI. After that, the samples were submersed in 15 mL of suspension GO (2 mg/mL) for 1 hour. After that, the samples were washed with 300 mL of distilled water under stirring for 24h. This procedure corresponds to one cycle of deposition PEI/GO on the MS surface. This process was repeated through different number of layers deposition. It was investigated the number of layers to achieve a fully cover by GO of the MS surface. With the maximum of 3 layers it was observed the significant increase of the total mass of PEI/GO on MS surface (Figure 33).

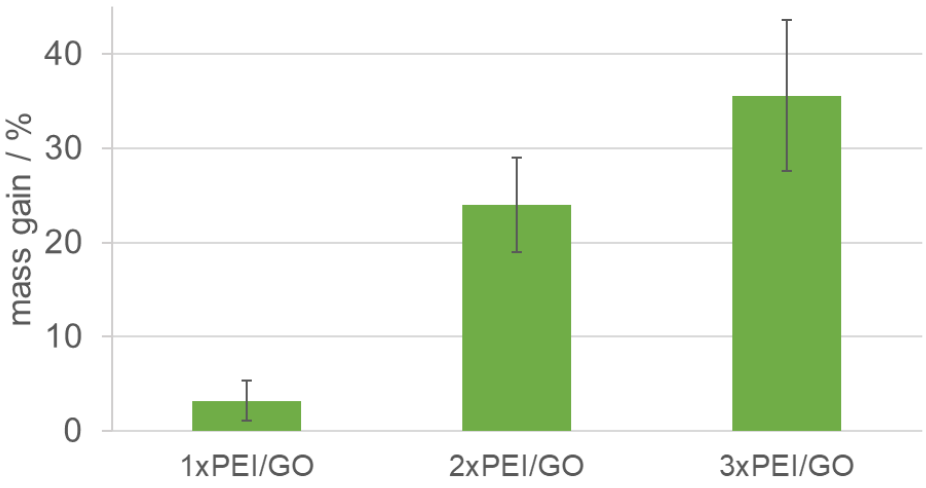

Figure 33. Mass gain of the MS with different 1, 2 and 3 of LBL cycles PEI/GO. Each value was calculated by the measurement of 5 specimens.

The assembly showed that, with just one layer of PEI/GO the scaffold was heavier than the original by the average value of 3.2± 2.1%. With the two layers of PEI/GO the mass significantly increases up to average value of 24.0±5.0%.

With the three layers of PEI/GO, there was a considerable mass gain of about 35.0±8.1%. This increase is due to the relation of cationic PEI and the negative charge of GO. With the increase of the number of PEI layers, there are more possibility to interact with the GO, and with this, improving the coverage of the MS. This coverage can be observed by SEM, where the MS pores are filled with the GO nanosheets (Figure 34). With the increase of the number of layers, a higher coverage is clearly observed. When the MS is covered with three layers of GO/PEI, it was observed that the mass gain is quite similar to the mass achieved for the two layers coverage. These results suggest that with three consecutive cycles the MS skeleton reaches a point of almost saturation for the accommodation of GO.

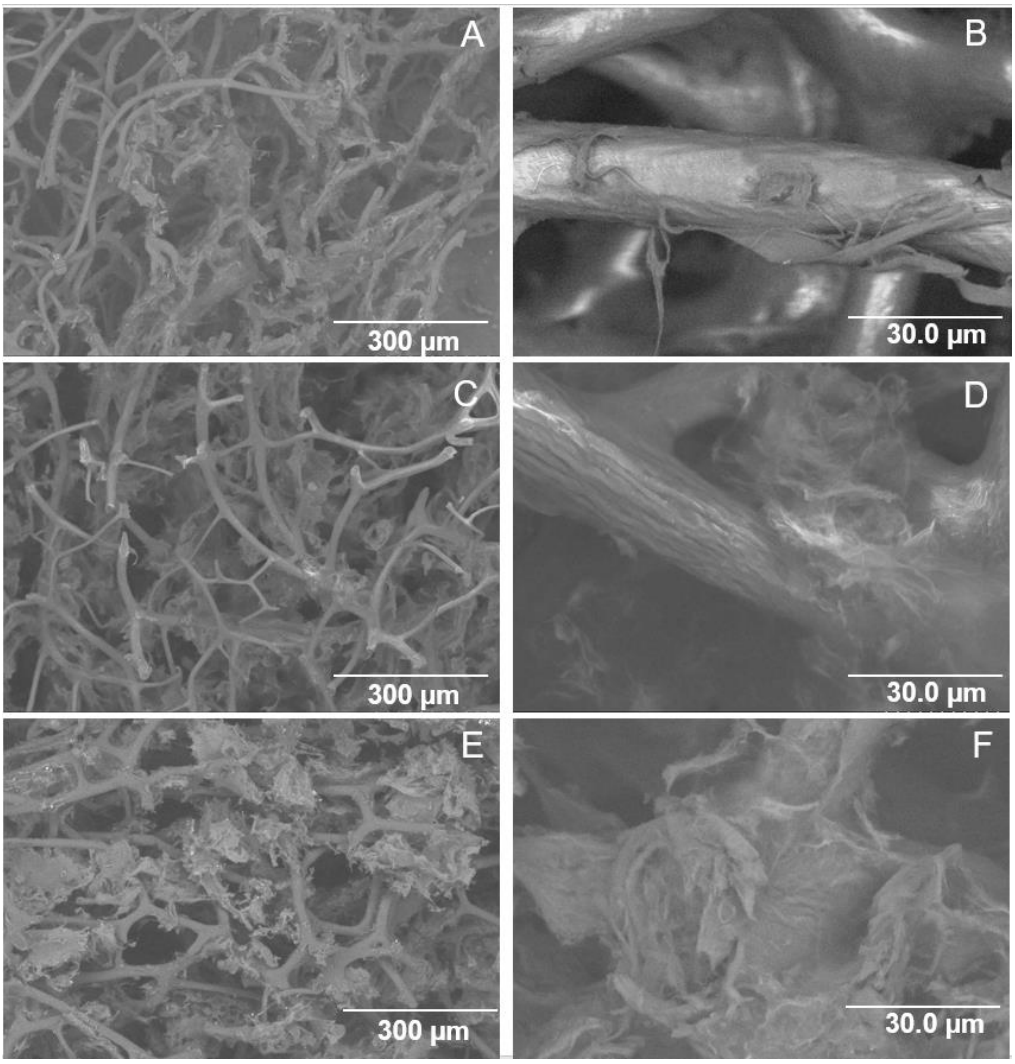

Figure 34. SEM images of a sponge with one (A,B) two (C,D) and three (E,F) layers of LBL assembly.

FTIR analysis was used to find the chemical characteristics of the nanocomposite materials MS/GO (Figure 35).

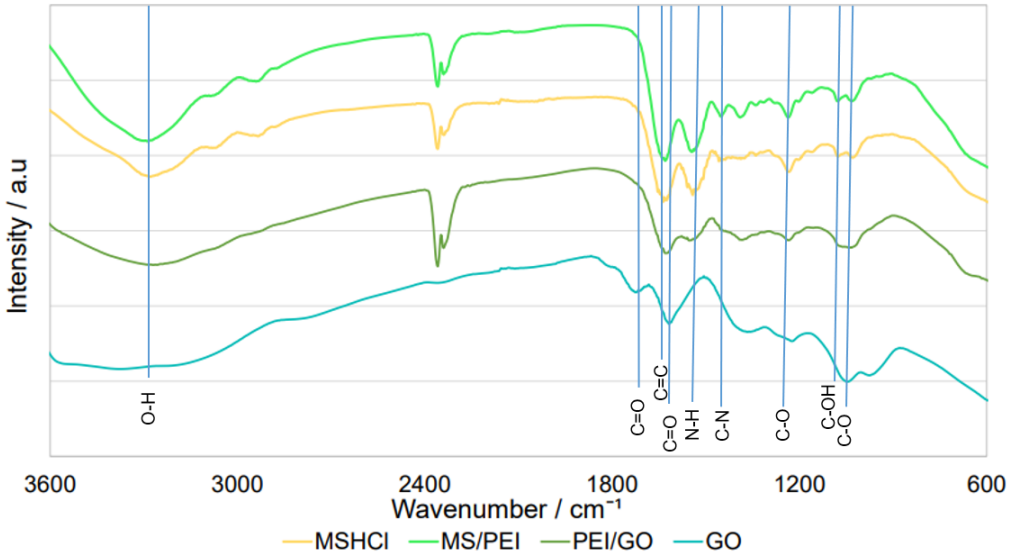

Figure 35. FTIR analysis of the scaffold using three layers deposition of PEI/GO.

Besides the MS peaks, FTIR analysis of the scaffolds presented some peaks related to presence of GO. As shown in Figure 35, the broad peak in the frequency range of 3200–3500 cm^{-1} is attributed to the O–H stretching vibration and the peak at 1151cm^{-1} ascribed to C-OH band, that related to the hydroxyl groups[78,79].Peaks like 1733 cm^{-1} is attributed to the C=O stretching vibration. Peak at 1633 cm^{-1} corresponds to the C=C stretching vibration, that are related to double bonds polycyclic aromatic rings[78–80]. The peak at 1385 cm^{-1} arises from the vibration of O–H groups. The absorption peak located at 1078 ascribed to epoxy C-O-C. Peak at 1050 cm^{-1} is related to alkoxy C–O stretching vibrations[79,80].The decrease of intensity of the epoxy C-O represented by the peak at 1232 cm^{-1} is due to the reaction of amine groups of PEI and the epoxy groups of GO, therefore confirming the successful incorporation of PEI and GO[81].

To investigate the structural stability of the new scaffold prepared with different layers of PEI/GO, several compression tests were performed. The obtained Young modulus of the scaffolds are similar to the sponge without any modification (Figure 36). Moreover, these results also suggest that the surface modification of the MS with different layers of PEI/GO did not affect the values of Young modulus. For the non-modified scaffold, the value of Young modulus observed was 0.177±0.066 MPa, after one layer deposition of PEI/GO was observed a value of Young modulus of 0.180±0.031 MPa, for two layers PEI/GO

deposition it was observed a value of 171±0.024MPa and for three layers PEI/GO it was observed a value of 0.176±0.027 MPa.

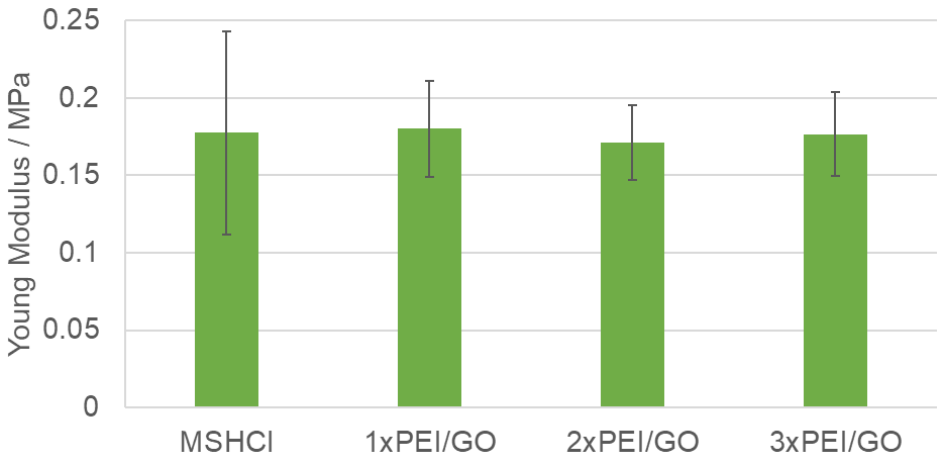

Figure 36. Young modulus of the MS scaffold modified with one, two or three layers of PEI/GO. Each value was calculated by the measurement of 5 specimens.

These results suggest that the mechanical properties of the final scaffolds can be mainly attributed to the MS skeleton mechanical properties and is independent of the number of layers of PEI/GO deposited on its surface.

3.3.2. LbL assembly of GO on MS using poly(diallyldimethylammonium chloride) (PDDA)

PDDA is an organic polyamine polymer and is usually used as cationic polyelectrolyte[58,77].It is considered is a quaternary ammonium polymer[82].The amount of 12.5 mg of PDDA is diluted in 500 mL of distilled water to obtain a solution with concentration of 5 mg/mL. Then the obtained solution was conserved in the fridge.

The sponge samples were submersed in 15 mL of PDDA solution, being removed all the air inside, and stirred for one hour. Then, the sponges were placed in 300 mL of distilled water and stirred for 30 minutes to remove the excess of PDDA. Samples were submersed in 15 mL of GO (2 mg/mL) for an hour[83]. After that, the samples were washed with 300 mL of distilled water for 24 h finishing the cycle, being used at least five samples for each batch. This protocol was considered one deposition layer of PDDA/GO on the MS surface.As reported for PEI, the PDDA/GO LbL technique was repeated until reach three times to validate the full coverage of MS surface.

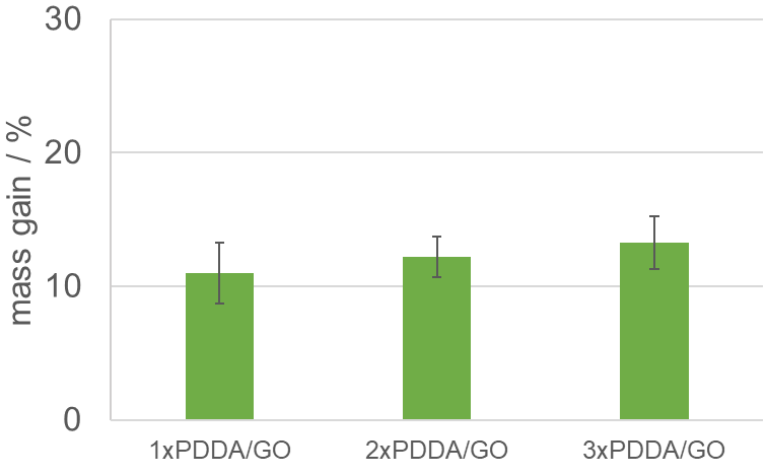

Figure 37. Mass gain using different number of PDDA/GO layers on the surface of the MS. Each value was calculated by the measurement of 5 specimens.

The Figure 37 show the total mass gain of the MS with different numbers of layers PDDA/GO explored is this work. It was observed a gradual mass gain from one (11.0±2.3%), two (13.0±1.5%) and three layers (14.0±1.9%) of PDDA/GO.

The coverage was not completely uniform, and when compared with the results obtained with the system PEI/GO it showed a significative loose in the efficiency for the MS surface coverage.

The coverage efficiency of the MS with GO using this polyelectrolyte can be analyzed by the SEM images of the different number of layers PDDA/GO showed in the Figure 38.

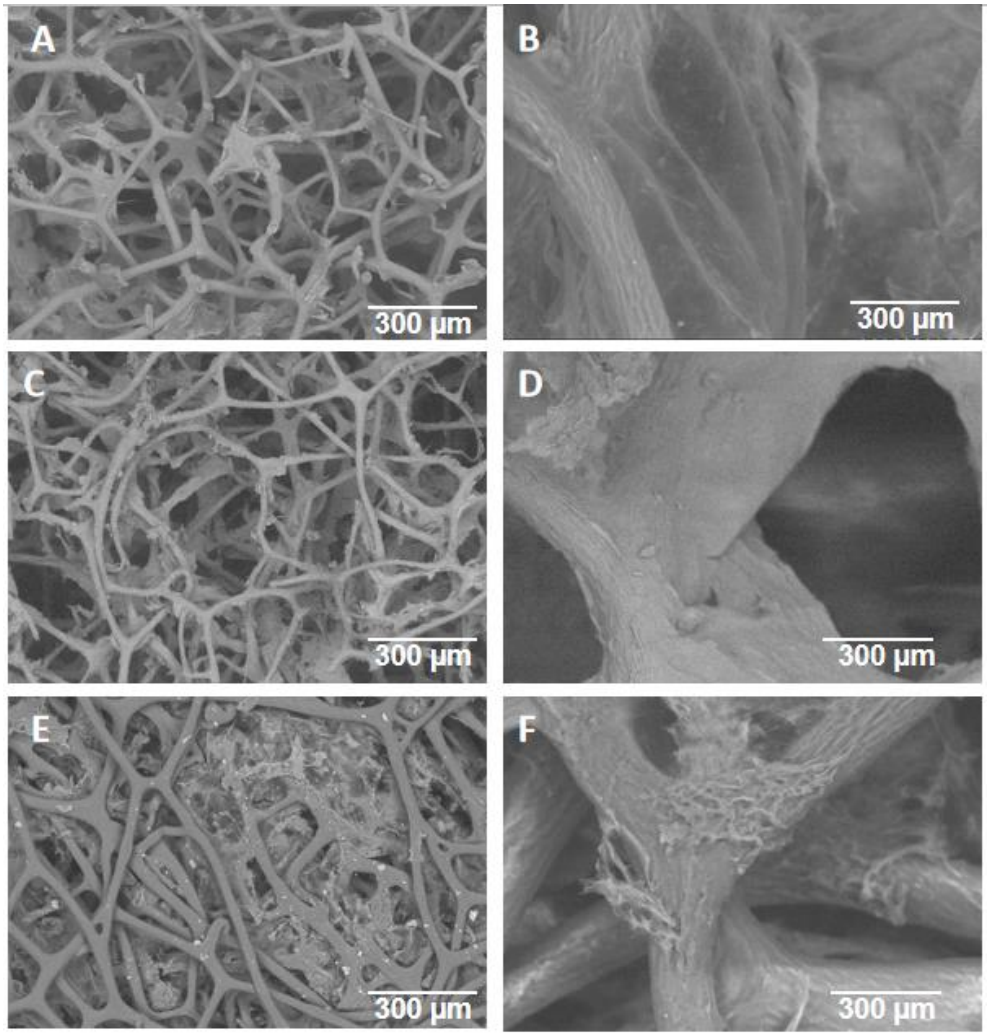

Figure 38. SEM images of a sponge with one (A, B), two (C, D) and three layers (E, F) of PDDA/GO.

With the number of layers of polyelectrolytes, the coverage is more effective, showing cloudy shadows in the SEM Images. With the increase of layers, it is possible to observe that some of the pores are covered by the GO nanosheets. However, as observed before for the % of gain of mass, the use of PDDA polyelectrolyte is less effective in the capacity of MS coverage. It resulted in a non-regular coverage of the fibers, and some agglomerations in the pores. These

results can be attributed to the less affinity of PDDA to the MS surface or GO. However, it also important to mention that the high molecular weight of PEI chains when compared with PDDA can give an important contribute for the more homogeneous coverage of the MS observed in the first approach. As observed before the mechanical behavior of the scaffold prepared with different layers of PDDA/GO presents similar values of Young modulus when, compared to the sponge without any coverage (Figure 39).

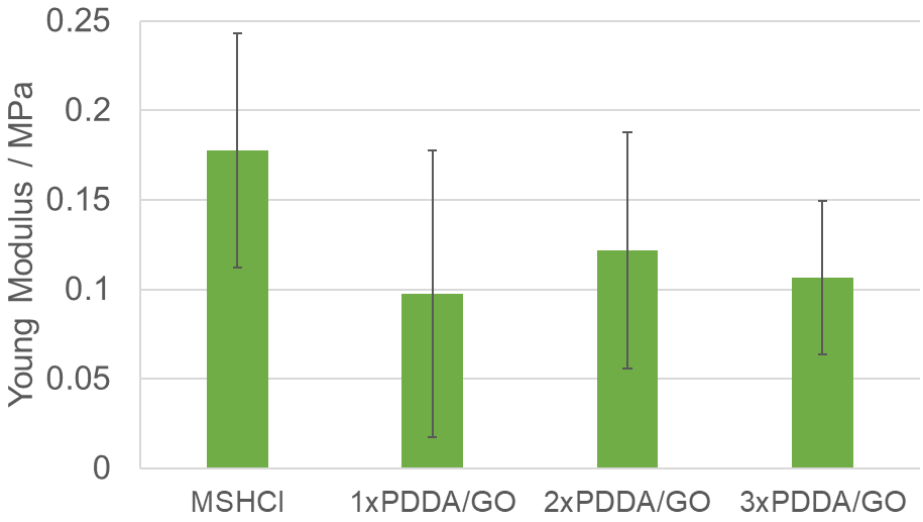

Figure 39. Young modulus of the MSHCl sponges modified with different layers of PDDA/GO. Each value was calculated by the measurement of 5 specimens.

As seen with PEI/GO scaffolds, the Young modulus using PDDA/GO depends mainly in the morphology and density of the sponge matrix. Young modulus of the scaffold has slight decreased comparing to the rest of the materials studied so far: 0.974±0.08 MPa, 0.121±0.067 MPa and 105±0.106 MPa for the 1xPDDA/GO, 2xPDDA/GO and 3xPDDA/GO, respectively. This slight decrease of Young modulus should be mainly attributed to the variability of sponge matrix morphology than to the less efficient coverage of its surface by the PDDA/GO, while the addition of the polyelectrolyte does not harm the original matrix and its mechanical behavior.

FTIR analysis of the scaffold modified with PDDA are shown in Figure 40. The peaks at 1222 cm^{-1} for C–O (epoxy) stretching and peaks at 1621 $cm^{-1}$of O–H groups, peaks at 2934 cm^{-1} and at 1466cm^{-1} ascribed to CH_n and C=C bonds,

respectively, represent some characteristics bonds that confirms the presence of PDDA[84,85].Other peaks like the broad peak in the frequency range of 3200–3500cm^{-1} is attributed to the O–H stretching vibration and the peak at 1151cm^{-1} ascribed to C-OH band, that related to the hydroxyl groups[78,80], are related to the presence of GO in the scaffold[78,80].

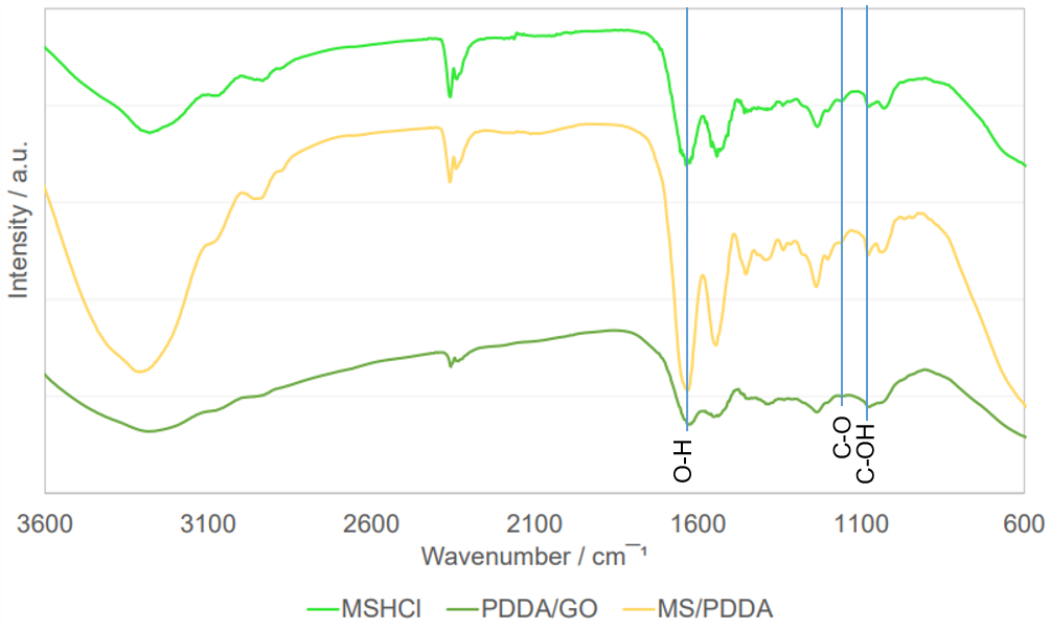

Figure 40. FTIR analysis of the MSHCl modified with three layers of PDDA/GO.

3.3.3. LbL assembly of GO using PDDA and PEI

In order to further investigate how the application of the polyelectrolytes influenced the sponge's coverage. The approach was followed: first the MS was covered with one layer of PEI/GO, and secondly with PDDA/GO as the second cationic intermediate layer (PEI/GO/PDDA/GO) defined as approach A (Figure 41A). the second scaffold was developed by the inverse order of polyelectrolytes used (PDDA/GO/PEI/GO) defined as approach B (Figure 41B).

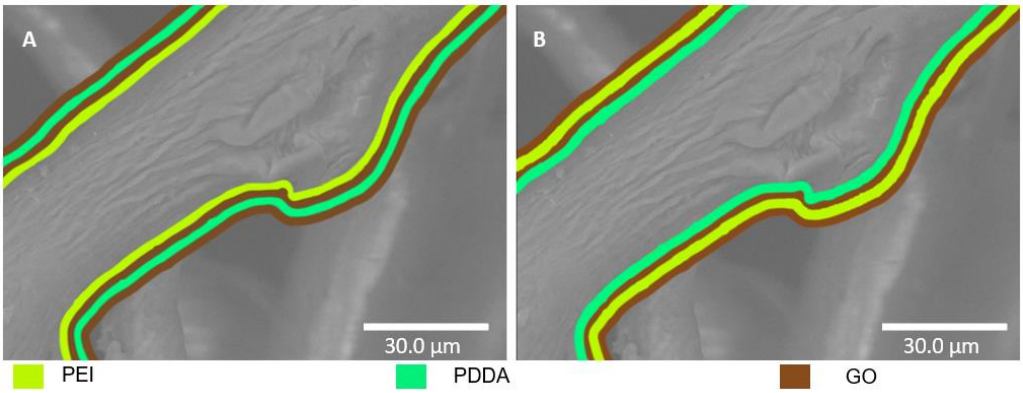

Figure 41. Schematic representation of the hybrid scaffolds produced by LbL using A) PEI/GO/PDDA/GO or B) PDDA/GO/PEI/GO.

With these different strategies two scaffolds with different mass gain and quality in the coverage yield were prepared (Figure 42).

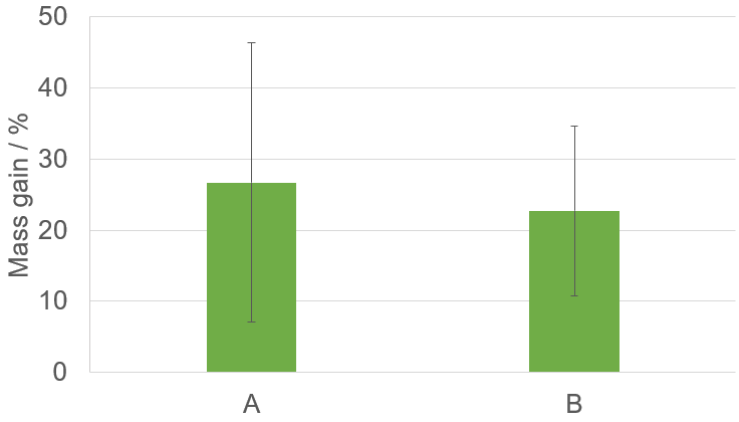

Figure 42. Mass gain with the different order of polyelectrolytes used on the LBL deposition:) PEI/GO/PDDA/GO or B) PDDA/GO/PEI/GO. Each value was calculated by the measurement of 5 specimens.

The difference of mass gain was expected because of the outcomes presented previously. The material used on the first layer set the yield of the coverage of the second layer. PEI tends to be more efficient in the coverage of the sponge (~27%) and, when used in the first application, the amount of material added to the scaffolds is higher comparing to the B process (~23%)[82]. With the use of both materials showed weaker results compared with the use of only one material (Figure 43).

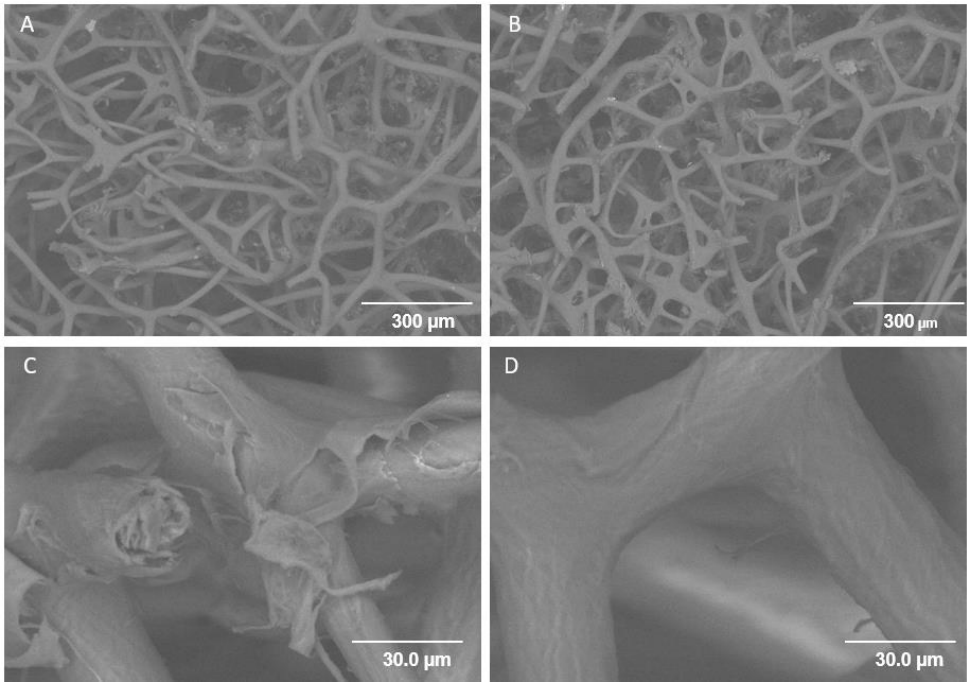

Figure 43. SEM images of hybrid scaffolds by the process A(A,C) and process B (B,D).

As seen before, there is a good adhesion of polyelectrolytes and GO to the sponge surface, where it is possible to see the development of a GO mesh in the different fibers of the sponge. The scaffolds that experienced the approach A, the formation of GO aggregates are more evident than when the approach B was used. To highlight that, after an intense wash of these scaffolds, GO remain attached to MSHCl surface in both cases.

As seen in the FTIR analysis of the samples, when only one type of polyelectrolytes was used, the characteristics bonds of all the components are present. However, this system is even more complex and the analysis of the presence of these bonds correspondent to each individual element in the hybrid scaffolds becomes more difficult (Figure 44).

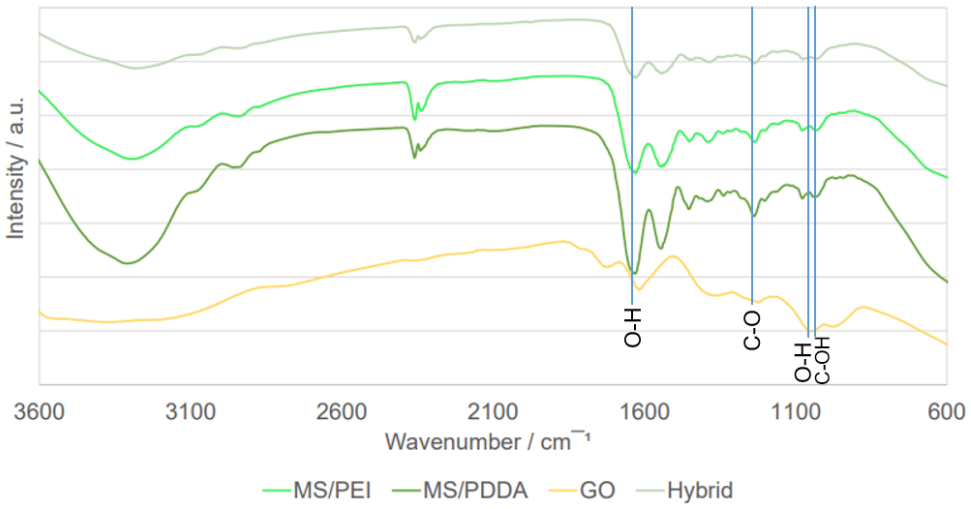

Figure 44. FTIR analysis of Hybrid scaffolds of MS/GO.

The hybrid scaffolds present many peaks that can represent any of the individual components, since these materials have some chemical bonds in common for PDDA, PEI and GO like C-O, O-H or C-OH, represented by the epoxy and hydroxyl groups present in the polyelectrolytes, and are the principal bonds for the presence of GO[82,83,85,86].

With these results obtained by LBL modification of the sponge's surface with GO, the scaffolds with more potential to have positive outcomes corresponds to the nanocomposite 3xPEI/GO, because it allows a uniform coverage of the sponge surface. Besides, it creates a sort of mesh between the fiber, that can be benefic for the cells seeding[82,83,86].

3.3.4. Thermal treatment of the scaffolds 3xPEI/GO

The scaffolds prepared by three LBL cycles of PEI/GO were tested for reduction by thermal treatment. The thermal treatment of 3xPEI/GO scaffolds was performed at 180ºC for 12 h under vacuum. The color modification of scaffolds from brown to black indicate the reduction of GO (Figure 45). With the increase of temperature, the mass of scaffolds decreased in about 23% of its original weight, before the LBL. These results can be mainly attributed to the release of oxygen and carbon from GO surface in the form of CO and CO_2 and evaporation of the adsorbed water[48].

Figure 45. Image of the (A) 3xPEI/GO and (B) 3xPEI/rGO scaffolds with thermal treatment at 180º C under vacuum (12h).

After this thermal treatment, the scaffolds were analyzed by SEM to investigate how its structure was affected (Figure 46). With the thermal treatment, the sponges still presented a uniform coverage of its fibers with rGO and keep the respective meshes between them. However, it was observed that the scaffolds presented a denser structure, reducing pores size and in some locations the rGO fully covered these gaps between the fibers.

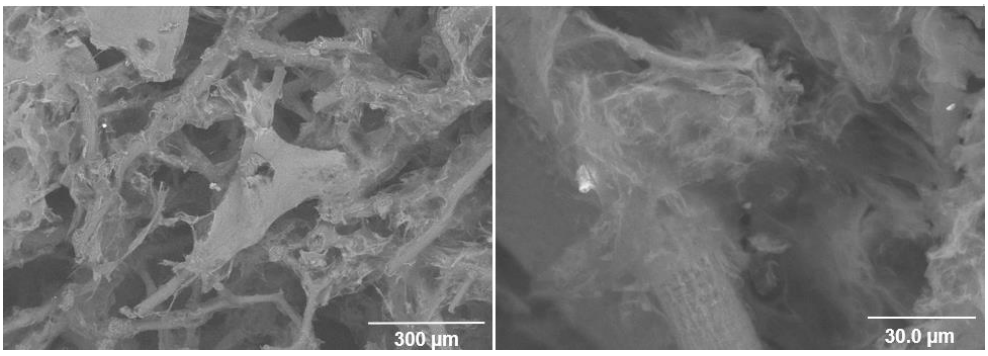

Figure 46. SEM images of the thermal treated 3xPEI/rGO at different magnifications.

FTIR analysis of the 3xPEI/rGO confirms the presence of rGO, when comparing to scaffolds 3xPEI/GO without heat treatment (Figure 47).

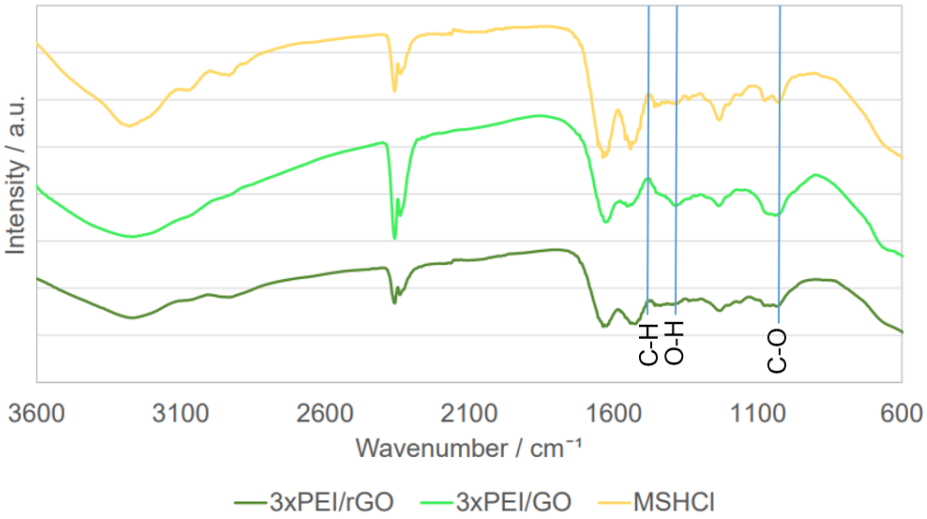

Figure 47. FTIR analysis of the thermal treated sponge(3xPEI/rGO).

In the FTIR analysis, is possible to observe a decrease of the peak intensity at 3420 cm^{-1} that corresponds to removal of -OH and at 1466 cm^{-1} which indicate a decomposition of the carbonyl groups[79,87]. The other peaks presented in the spetra show that its chemical composition of the MS stays unchanged with the heat treatment, as observed in our results reported previously for the heat treatment of the MS under the same experimental conditions.

After the reduction of GO, the compression tests were performed to compare with the ones done with the samples without thermal treatment studied before (Figure 48).

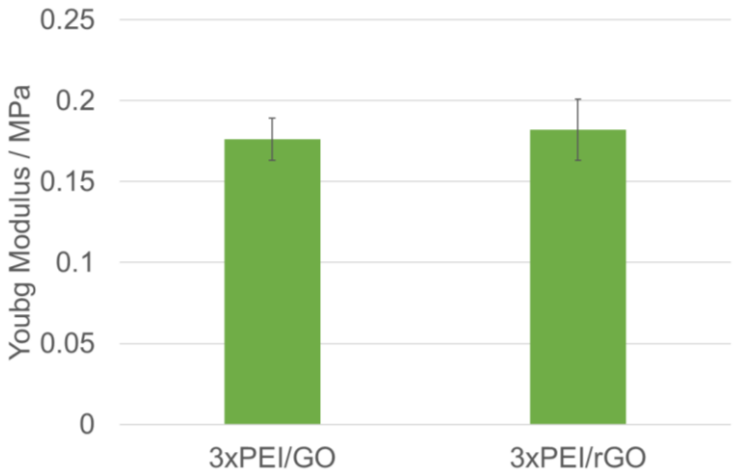

Figure 48. Young Modulus of 3xPEI/GO and 3xPEI/rGO. The values are obtained from the measurement of 5 specimens.

With this treatment, 3xPEI/rGO samples showed that young modulus values (0.182±0.019 MPa) were similar with 3xPEI/GO samples representing about 0.176±0.019 MPa. As seen with the sponge without the addition of GO, the increase of temperature resulted in denaturation of proteins and densification of the fibers, but its mechanical properties remained[88].

With these experiments with different approaches to obtain self-assembled scaffolds, the most crucial material is the sponge, because all the mechanical properties rely on its physical and chemical characteristics. As reported, GO and rGO are materials that can provide better outcomes when in contact with different cells as they can act as conductive, antibacterial, osteogenic agents and are able to deliver drugs[87,89], so these samples were tested with osteoblastic cells to study their behavior in this environment under *in vitro* static and dynamic compression tests.

CHAPTER 4

4. *In vitro* tests of the MS/PEI/GO scaffolds

4.1. Materials and methods

4.1.1. Cell seeding

The scaffolds were seeded with an osteoblastic cell line MC3T3-E1 (ATCC CRL-2593). These cells were maintained at 37 °C in a moisture atmosphere of 5% CO_2 and air, in a L-glutamine and sodium pyruvate containing Alpha Minimum Essential Medium (α-MEM, Sigma-Aldrich) that was supplemented with 10% (v/v) fetal bovine serum (FBS, Sigma-Aldrich), 1% (v/v) penicillin/streptomycin solution (containing 10,000 units penicillin and 10 mg streptomycin/mL) (Sigma-Aldrich), and 2.2 g/L Sodium Bicarbonate ($NaHCO_3$, Sigma Aldrich. Cells were harvested at pre-confluence using 0.25% trypsin/EDTA solution (Sigma-Aldrich). These cells were seeded in three types of scaffolds: being the control the MSHCl sponge, sponge with the deposition of three layers of PEI/GO by LbL technique(3xPEI/GO), and the reduced counterpart with thermal treatment (3xPEI/rGO). Before cell seeding, all scaffolds were sterilized two times in 70% (v/v) ethanol aqueous solution for 4 hours, washed in Phosphate-Buffered Saline (PBS, 1x, Sigma-Aldrich) 3 times, placed in a 48-well plate (Figure 49). Then, MC3T3-E1 cells were seeded onto the scaffolds at an initial density of 10,000 cells/scaffold, followed by an incubation at 37 °C for 2 hours. Afterwards, fresh medium was added to the scaffolds and, cell-seeded scaffolds were cultured for 28 days, with two medium changes for week.

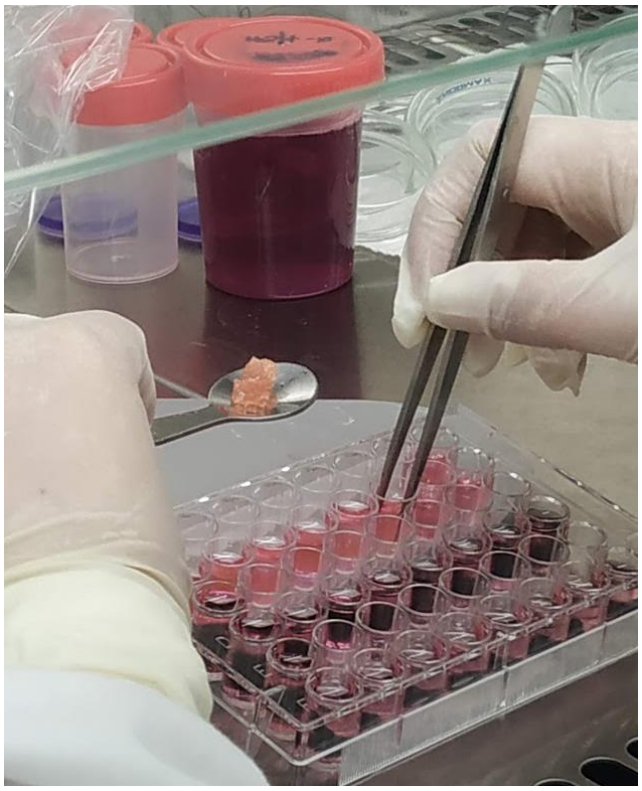

Figure 49. Seeding of the MC3T3-E1 cells in the scaffolds MSHCl, 3xPEI/GO and 3xPEI/RGO.

4.1.2. Incubation of cell-laden scaffolds into the bioreactor

After an initial attachment period of 7 days, 4 cell-laden scaffolds of each composition were placed in the bioreactor (Figure 50) and subjected to unconfined compression on a developed bioreactor[90]: 2 hours of sinusoidal compression (0.5 Hz, 0-10 % strain) and 4 hours of rest, 4 times a day for 14 days. A 4 static controls were placed and cultured in the incubator for the 14 days.

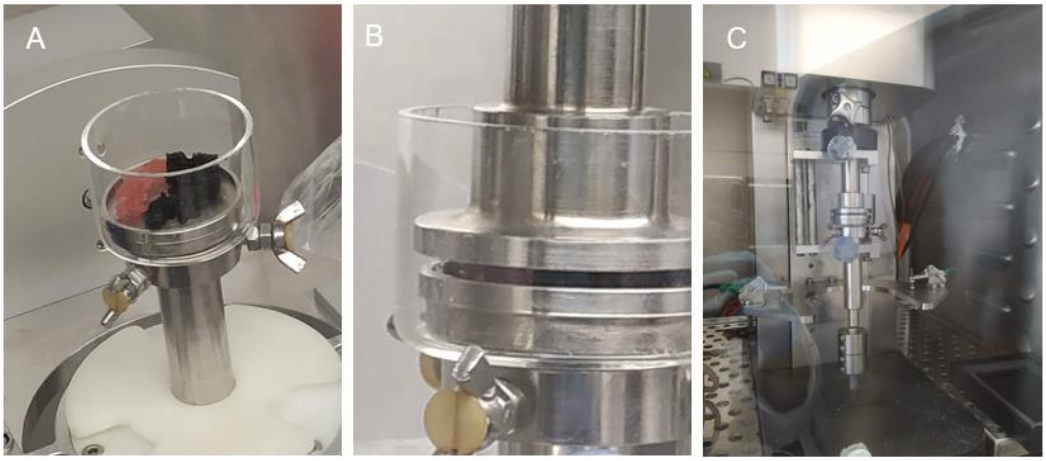

Figure 50. Implementation of the different scaffolds (MSHCl, 3xPEI/GO and 3xPEI/rGO) on the bioreactor for the dynamic cell culture tests.

4.1.3. Metabolic Activity

After 1, 7, 14 and 21 days of culture, cell metabolic activity was calculated based on the resazurin method. A resazurin solution (0.1 mg/mL in PBS; ACROS Organics) was added to fresh medium with a final concentration of 10% (v/v). Scaffolds were incubated in this solution at 37 ºC for 4 hours in the dark, after which triplicates of 100 µL per well for three times were transferred to a 96-well plate and absorbance at 570 and 600 nm was measured. The absorbance values of the negative control (scaffold without cell seeding) were subtracted to the final value. The absorbance values of the same number of cells incubated in the tissue culture polystyrene (TCPS) on the first time point were taken as 100% and cell viability calculated as a percentage of these control values.

The resazurin method that is a photometric test that assesses cellular metabolic activity through the reduction of resazurin (7-hydroxy-3H-phenoxazin-3-one10-oxide), a blue non-fluorescent reagent into resorufin which is highly fluorescent and pink in color. This conversion triggered by dehydrogenase of metabolic active cells in response to changes of the reducing environment within the cytosol of the cell, is proportional to the number of viable cells in the sample, and it can be quantified using a spectrophotometer at the 570 and 600 nm, which correspond to the maximum resazurin absorbance and the maximum resorufin absorbance, respectively[91,92].

4.1.4. Mineralization assay

After the culture, the medium where the samples were submersed was aspired and then the samples were rinsed with PBS and fixed in 4% paraformaldehyde/PBS for 20 min at room temperature. After the fixation, samples were permeabilized with 0.1% Triton X-100/PBS for 5 min and further rinsed for 5 min three times in PBS[93].400 µL of 40 mM Alizarin Red S (ARS) was added to each well to stain the calcium deposits during agitation for 20 min with an orbital shaker (100 rpm). The ARS was aspirated, and the plates were washed with milliQ water.

For quantification of staining, 400 µL of 0.1 M cetylpyridinium chloride was added to the stained samples for 1 hour under agitation with an orbital shaker to release the ARS staining from the cell matrix. A 96-well plate was filled with 100 µL of the remaining supernatant to be read at 570 nm with a plate reader.

4.1.5. Preparation of samples for cell morphology analysis

Samples were fixated as previously described, using the 4% paraformaldehyde solution in PBS (ACROS Organics). Samples were then washed with PBS for 3 times. The PBS was then replaced by a solution with ethanol concentration of 50% to start the dehydration process. This process was repeated with the increase of ethanol concentration, of 70, 90, 95 and 100% v/v ethanol (Panreac AppliChem).

In order to dry the samples, they were transferred from the last ethanol solution, of 100% concentration to a 1:2 solution of hexamethyldisilazane (HMDS)(TCI): 100% ethanol where they stood for 20 minutes. They were then transferred to a 2:1 solution of HMDS: 100% ethanol for 20 minutes. At last, samples were transferred to a 100% HMDS for 20 minutes, and then this solution was removed and the scaffolds were left overnight with the lid open in a fume hood for air drying[94]. Scaffolds were then mounted in an aluminum stub and visualized by SEM.

4.2. Biocompatibility studies of the scaffolds

The percentage of the viable cells on the scaffolds at days 1, 7, 14 and 21 of culture is shown at Figure 51. After 1 day of culture, a beneficial impact on cell attachment was observed on the compositions containing GO[87,89,95], since the control (MSHCl) displayed the lowest percentage of viable cells – 25%, while 3xPEI/GO and 3xPEI/rGO displayed substantially higher percentage of viable cells –56 and 57%, respectively. This behavior has been previously reported and attributed to the GO's hydroxyl groups that promotes cell recruitment and attachment to the surface[11,87,89,95].

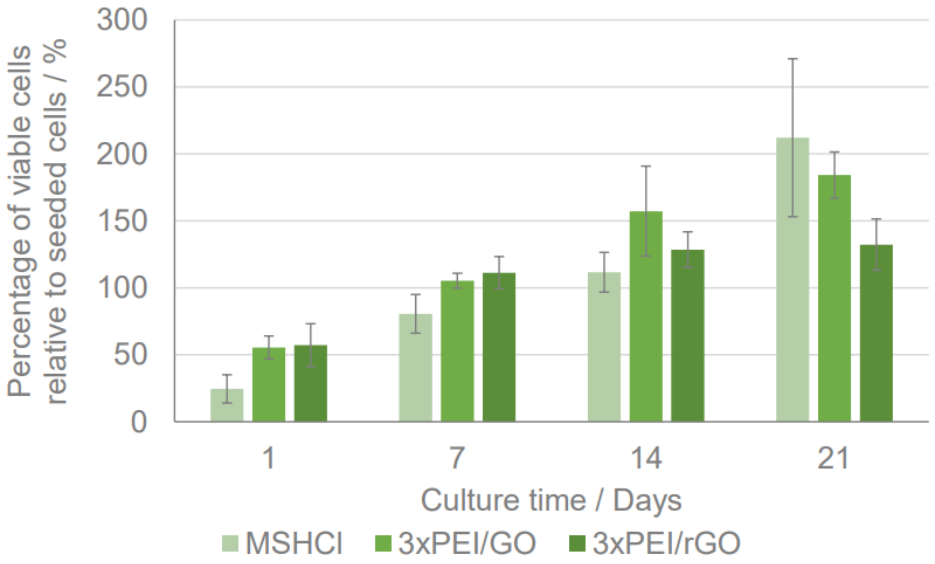

Figure 51. Cell viability studies with the different scaffolds studied using static conditions.

After 7 days of culture, an increase on the viability was observed, regardless of the types of scaffold (81%, 105% and 111% for MSHCl, 3xPEI/GO and 3xPEI/rGO, respectively), implying that cell proliferation occurred. This behavior was consistently detected throughout the culture period, suggesting that the MSHCl, as well as the GBM counterparts, have low toxicity and are biocompatible[26,31,96].

Interestingly, while at day 7 small differences were observed between the GBM-based compositions, as observed at day 1. By day 14 a substantial increase on viability was observed for the 3xPEI/GO (157%) in comparison with the other compositions (111% and 128% for MSHCl and 3xPEI/rGO, respectively)[89]. Still,

between the last two time points (14 and 21 days), no differences were observed on the GBM-based compositions, specially with 3xPEI/GO (184% and 132% for 3xPEI/GO and 3xPEI/rGO, respectively), while a considerable rise on the percentage of viable cells was detected on the control (212%)[31]. Both of these samples also present PEI, as it is reported having an excellent biocompability[76]. It is possible that a slight reduction of the GBM coverage due to its degradation, and a consequent cell loss, might have caused this phenomenon on the GBM-based compositions[97].

Figure 52 shows the percentage of the viable cells on the scaffolds after 21 days of culture under static and dynamically compression conditions. Upon the application of mechanical stimulation, the percentage of viable cells on the scaffolds was substantially higher (301%, 260% and 204% for MSHCl, 3xPEI/GO and 3xPEI/rGO, respectively), suggesting that the dynamic environment positively influenced cell proliferation[54,98]. This behavior has been previously reported[54]. With the compression applied to the scaffolds, it could result in the detachment of the coverage from the scaffold, and consequently, the removal of osteoblastic cells from the body of the scaffold.

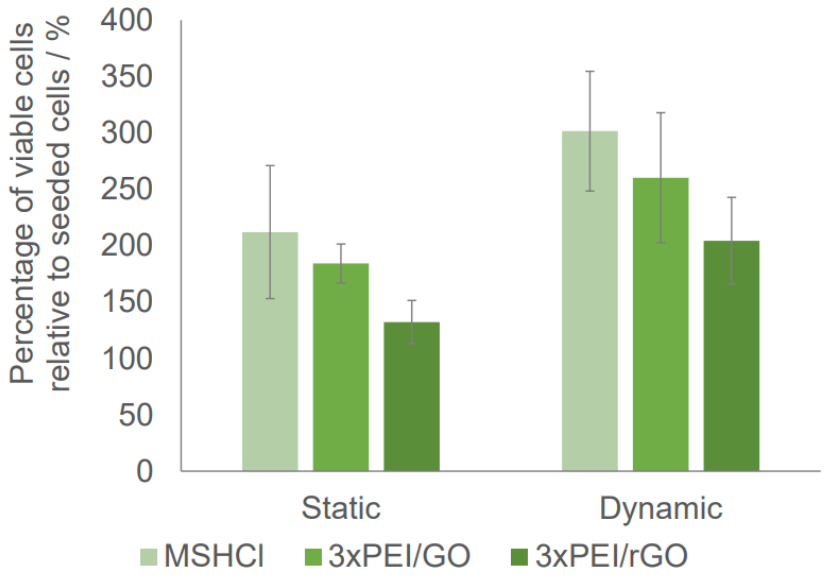

Figure 52. Cell viability studies of the scaffolds under static and dynamically compressed conditions at day 21.

It is concluded that both MS and GBM are not harmful for the osteoblastic cells, showing a good proliferation in all cases. When cells are in touch with the new materials with GO composites, it shows that the use of the GO induces more adhesion and multiplication of osteoblastic cells, comparing to rGO scaffolds. GO is highly oxidized and because of the presence of functional groups in their sheet provided the linking with cells[99]. The reduction of GO is known to remove some of their functional groups, turning this material less hydrophilic than GO. This more hydrophobic features can lead to its aggregation on the cell membrane, turning it toxic to cells[100]. The reduction of the scaffold promote deterioration of some proteins of the MSHCl, that with the handling during the medium changes may led to the disaggregation of several cells being removed from the scaffold.

4.3. Biocompatibility studies of the scaffolds

Figure 53 displays the alizarin red mineralization rate on the MSHCl, 3xPEI/GO and 3xPEI/rGO scaffolds after 14 and 21 days of culture.

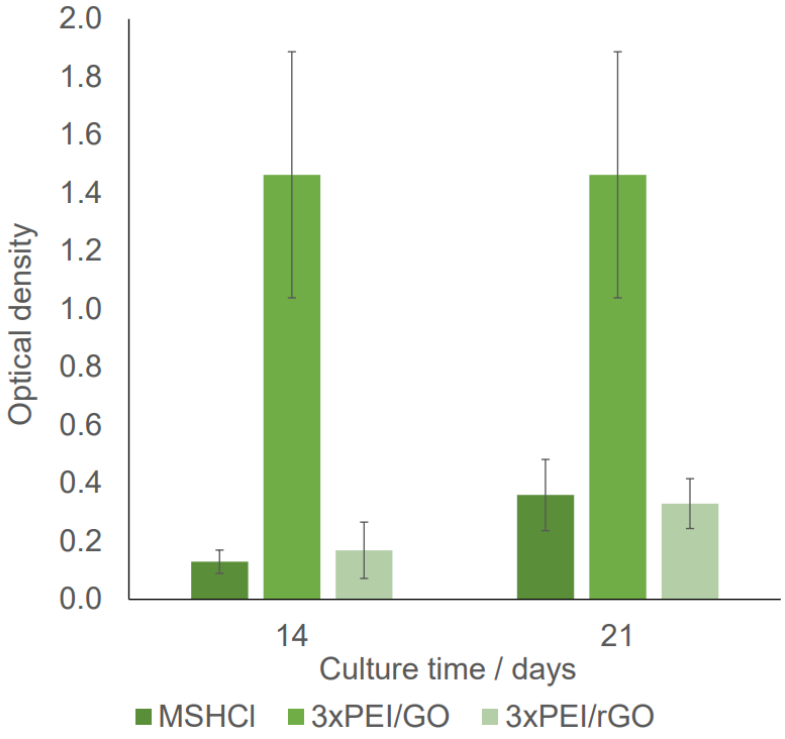

Figure 53. Mineralization studies of the MSHCl, 3xPEI/GO and 3xPEI/rGO scaffolds after 14 and 21 days of culture determined using Alizarin red staining assay.

A clearly higher mineralization rate was observed for the 3xPEI/GO composition after 14 days of culture (1.5) in comparison with MSHCl (0.13) and

3xPEI/rGO (0.17). A similar behavior was also detected at day 21. Still, an increase on the mineralization rate was observed over time for the MSHCl (0.36) and 3xPEI/rGO (0.33). The presence of GBM showed a higher increase of mineralization of the ECM.

Regarding the mechanical stimulation, higher mineralization rates were observed after dynamic compression of the cell-seeded scaffolds, regardless of the composition (0.59, 2.16 and 0.76 for MSHCl, 3xPEI/GO and 3xPEI/rGO, respectively), which is consistent with previous reports[54,98,101,102].

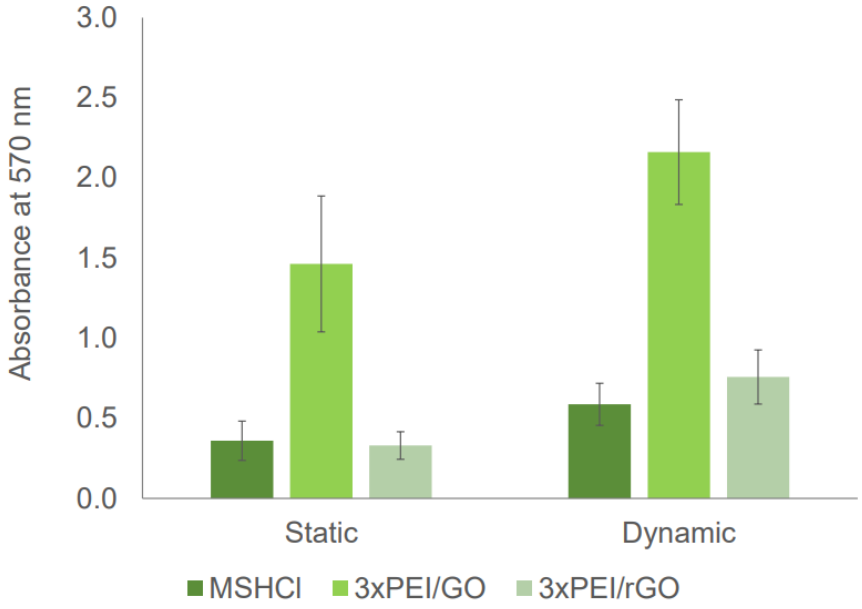

Figure 54. Mineralization studies of the MSHCl, 3xPEI/GO and 3xPEI/rGO scaffolds after 21 days of culture under static and dynamically compressed conditions.

Here again, a higher absorbance was obtained for the 3xPEI/GO composition, suggesting that this composition might have a beneficial impact on extracellular matrix mineralization[92,93].

4.4. Cell morphology

Cell distribution was assessed through SEM visualization after 7, 14 and 21 days of culture (under static and dynamically compressed conditions). The SEM images of the cell-seeded scaffolds are shown in Figure 55, for 7 days of culture. Here, cells were visible in all compositions, including the control[103].

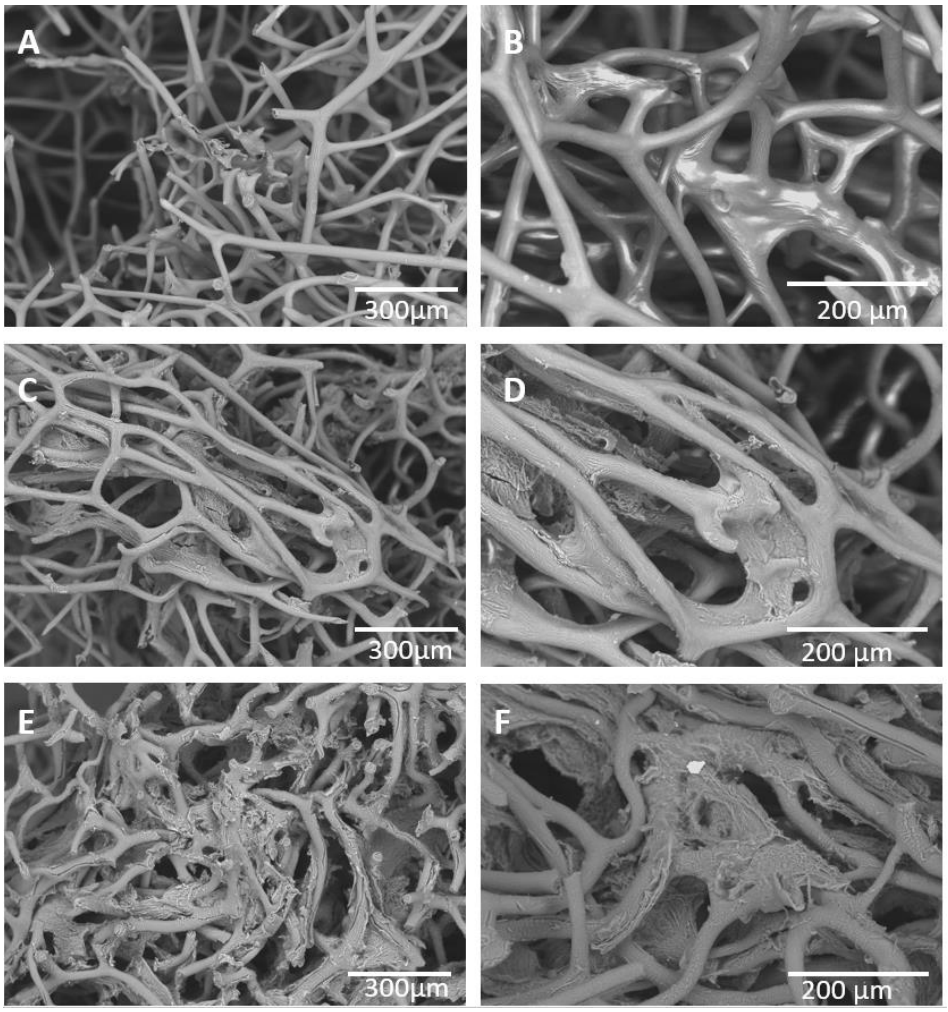

Figure 55. SEM image of the cell seeded scaffolds MSHCl (A, B), 3xPEI/GO (C, D) and 3xPEI/rGO (E, F) after 7 days of culture.

After 7 days of culture of MSHCl sample, it is possible to observe the formation of a cell ayer covering the fibers. In fact, when fibers channels are closed, cells formed bridges between them. Interestingly, the incorporation of GBMs enhanced the cell attachment since denser coverage of the fibers was visible[104]. These results are in agreement with the cell viability results previously reported[89,104]. The scaffold composition that showed better coverage was GO, which can be attributed to the presence of oxygen functional groups, making these composites more receptive to connect with cells[89,105].

The culture of cell-seeded scaffolds after 14 days of culture were studied by SEM images shown in Figure 56. These images are relatable to the ones taken at 7 days of culture, as all of them presented osteoblastic cells in its composition, as expected when observed the values for metabolic activity shown above.

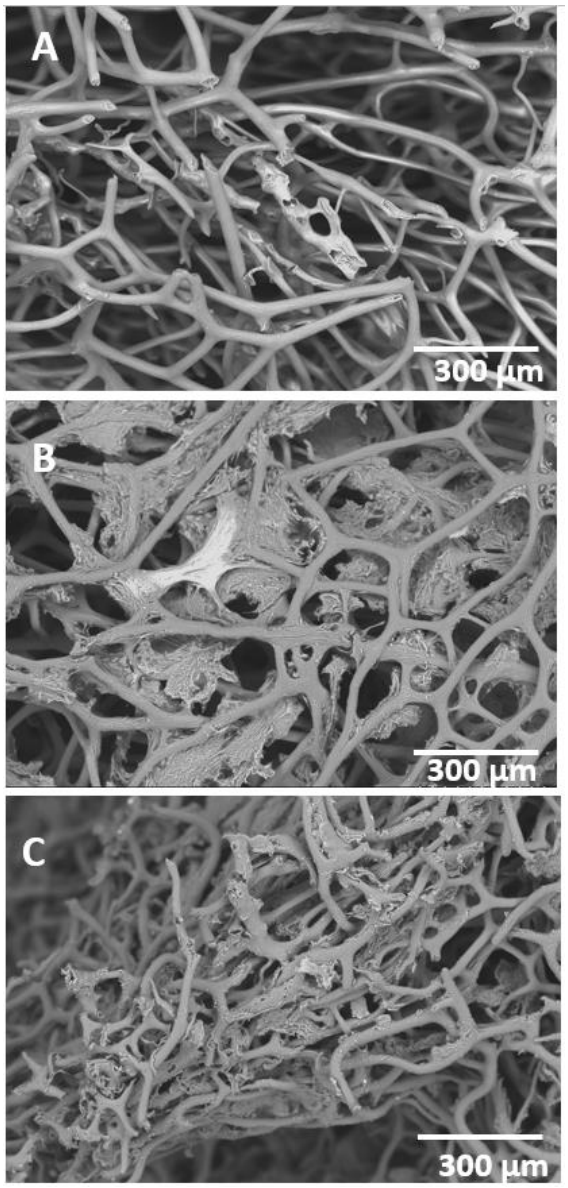

Figure 56. SEM image of the static scaffolds of MSHCl(A), 3xPEI/GO(B) and 3xPEI/rGO(C) studied at day 14.

When observing the GBM scaffolds, the amount of coverage by these products tends to decrease, comparing to the first images of the scaffold. This can be due to the long time of contact with water, and consequently, the deterioration of GO structure. However, the portions that have strong bonds with the scaffolds, cells show to grow and multiplication of cells, confirming that the use of this material turns the MS a positive environment for the osteoblastic cells to adhere and proliferate[106].

From the scaffolds incubated in the bioreactor, it can be observed the difference of cell adhesion in a dynamic (Figure 57A, 57C, 57D) and static medium (Figure 57B, 57D, 57F) at the 21st day.

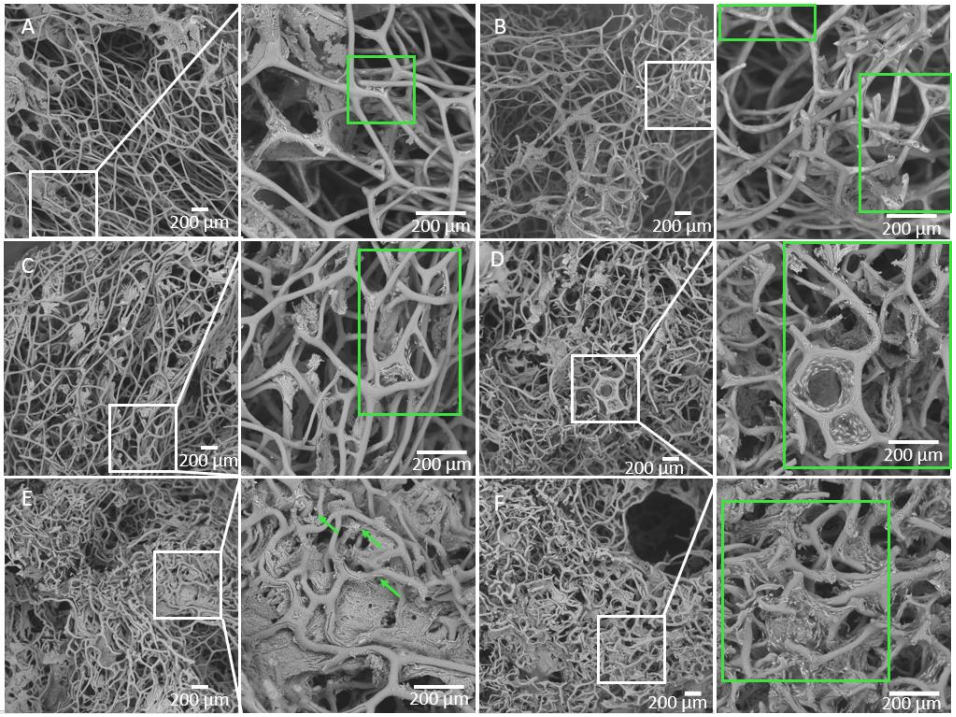

Figure 57. SEM of the cell-seeded scaffolds day 21 of culture in dynamically compressed for MSHCl(A), PEI/GO(C) and PEI/rGO (E) and MSHCl (B), PEI/GO (D) and PEI/rGO (F) in static environment.

Here, all the samples showed the presence of the osteoblastic cells in their fibers. Cells seem to adhere only where there is the presence of GO, confirming its ability to improve cell adhesion[51,107,108].With dynamic environment, the pressure applied on the scaffold, the way it is submersed in SBF and the contact for a long period of time, it may deteriorated the GO resulting in detachment from the MSHCl[101].

When comparing the cellular tests from these materials, it can be considered that the use of GBM has a beneficial impact, because with the use of these materials, there is an evolution of the metabolic activity of osteoblastic cells and the addition of GO and rGO shown to have a superior performance on extracellular matrix mineralization comparing to the control scaffold, which can translate in the better capacity for formation or renewal of the bone[92,93,109].

CHAPTER 5

5. Conclusion and future remarks

To achieve a better performance of the MS skeleton as a biomaterial matrix, the structure was firstly purified with two different methods. The acid treatment under soft conditions revealed to be the most effective to remove all the present inorganic impurities in the sponge. The results revealed that with the purification employed, the matrix of the original sponge was not damage and its chemical and mechanical properties were not affected.

The marine sponges skeleton have already showed to present some potential as scaffold for bone tissue engennering[110]. Here we intent to increase their potential by combining the high mechanical performance of the sponge matrix with the excellent properties of GBM in order to develop smart nanocomposites able to be mechanically stimulated. For that purpose, here was explored the self-assembly of the MS with GO by LbL approach. Self-assembly technique turned out to be very interesting approach as it provides a variable number of possible new materials. With the polyelectrolytes used, PEI shown to be the one with higher yield of coverage of the scaffold's matrix designed. The results showed that after three consecutive cycles PEI/GO it was observed a significant mass gain into the original MS matrix (35.0±8.1%). However, it was noticed that the number of cycles applied, and consequent mass gain did not affect the mechanical properties of the final nanocomposite materials, once the MS matrix is the main responsible for the mechanical performance. The three cycles deposition of PEI/GO on the surface of MS matrix showed a more homogeneous cover with significante rugosity, important to increase the scaffold's surface area and decrease the space between fibers which can be helpful to induce biocompatibility and proliferation of osteoblastic cells. With the different analysis made during the practical work of all sort of scaffolds, it is possible to conclude that LBL technique is effective as the main constituents of the materials are present in the nanocomposite's composition.

When temperature was used to obtain a new reduced counterpart of the nanocomposites (3xPEI/rGO), it was observed that the thermal treatment had an important impact on the structure of MS, as the sponge was densified. However, its chemical features was similar to the original samples. Moreover, the chemical analysis of the reduced nanocomposites showed that the thermal treatment at 180°C/12h under vacuum was very effective, since the concentration of oxygen decreases significantly. The mechanical properties of these new material is also mainly dependent of the MS matrix as it gives the scaffold all the structure and support, being that translated to its elastic properties.

The biocompatibility studies of the different nanocomposites (3xPEI/GO and 3xPEI/rGO) performed with the osteoblast cells under dynamic and static conditions, showed that all samples presented a very positive outcomes in terms of biocompatibility. After 7 days of static culture, an increase on the cell viability was observed, regardless of the composition (81%, 105% and 111% for MSHCL, 3xPEI/GO and 3xPEI/rGO, respectively), suggesting that the MSHCl, as well as the GBM counterparts, have low toxicity and are biocompatible. By day 14 a substantial increase on viability was observed for the 3xPEI/GO (157%) in comparison with the other compositions (111% and 128 % for MSHCL and 3xPEI/rGO, respectively). After 21 days significant differences were observed on the GBM-based compositions,184% and 132 % for 3xPEI/GO and 3xPEI/rGO, respectively, while a considerable rise on the percentage of viable cells was detected on the control (212%). Under dynamically compressed conditions. of the scaffolds, after 21 days of culture it was observed that the percentage of viable cells on the scaffolds was substantially higher,301%, 260% and 204% for MSHCl, 3xPEI/GO and 3xPEI/rGO, respectively, suggesting that the dynamic environment positively influenced cell proliferation. The lower values of the metabolic activity of the GBM comparing to the control may result from the loss of the GO coverage due to its degradation[97]. After prolonged water exposure, GO particle sizes tend to decrease over time due to the possible C-C bond cleavage[97]. With the medium change and handling, some cells that were adhered with the GO which some residual portions had detached from the matrix could translate in the decrease of the number of cells present in the scaffold. However, it was observed a higher mineralization rates after dynamic compression of the

cell-seeded scaffolds for the samples modified with GBM, 0.59, 2.16 and 0.76 for MSHCL, 3xPEI/GO and 3xPEI/rGO, respectively. The higher mineralization content of the samples showed that the use of GO resulted in a significant increase of Ca deposition which can be related to the bone formation, critical for the regeneration of new bone tissue.

The future direction of this research points to further clarification of the bone forming specificity from these scaffolds by animal studies. In vivo bone formation by these nanocomposites shall be tested in small and large animal models before promising to be a potential scaffold for tissue engineered bone regeneration.

A possible approach to study in the future would be the use of a marine sponge with thermal treatment with the coverage of GO, as the matrix will be denser, because of the increase of the diameter of the fibers, turning the inter-channel spaces smaller, which can be more beneficial to the creation of osteoblastic bridges in all scaffold. The addition of GO instead of rGO could increase the adhesion of the cells and turn the scaffold more stable, as it presents more functional groups in its composition, which can result in less detachment of the coverage, and consequently, higher cell viability. All these composites have to be tested in vitro, with different parameters such as the number of initial osteoblastic cells, the amount of time for cell seeding, and the parameters for dynamic stimulation

Another important feature of this materials that can be interesting to explore is their ability for the biodegradation and immunogenicity. In that sense, will be important to obtain significant insights regarding the study of the mechanisms of degradation of GBM over the mechanical stimulation on vitro osteoblastic cultures. The establishment of the parameters that can promote the degradation of the GBM/MS nanocomposites should be very relevant for the development of biodegradable scaffolds that can be degraded according to in vivo growth of the natural bone tissue.

6. References

1. Henkel J, Woodruff MA, Epari DR, et al. Bone Regeneration Based on Tissue Engineering Conceptions-A 21st Century Perspective. *Bone Res*. 2013;1:216-248. doi:10.4248/BR201303002

2. Qu H, Fu H, Han Z, Sun Y. Biomaterials for bone tissue engineering scaffolds: A review. *RSC Adv*. 2019;9(45):26252-26262. doi:10.1039/c9ra05214c

3. Amini AR, Laurencin CT, Nukavarapu SP. Bone tissue engineering: Recent advances and challenges. *Crit Rev Biomed Eng*. 2012;40(5):363-408. doi:10.1615/CritRevBiomedEng.v40.i5.10

4. Filippi M, Born G, Chaaban M, Scherberich A. Natural Polymeric Scaffolds in Bone Regeneration. *Front Bioeng Biotechnol*. 2020;8(May). doi:10.3389/fbioe.2020.00474

5. Aluma Y, Ilan M, Sherman D. Comments on a skeleton design paradigm for a demosponge. *J Struct Biol*. 2011;175(3):415-424. doi:10.1016/j.jsb.2011.05.006

6. Dubey N, Decroix FED, Rosa V. Graphene: An Emerging Carbon Nanomaterial for Bone Tissue Engineering. *Graphene based Mater Heal Environ*. 2016:135-158. doi:10.1007/978-3-319-45639-3_5

7. Almeida SS, Girão AF, Gonçalves G, Completo A, Marques PAAP. *Stimulus Responsive Graphene Scaffolds for Tissue Engineering*.; 2016. doi:10.1007/978-3-319-45639-3_8

8. Smith AT, LaChance AM, Zeng S, Liu B, Sun L. Synthesis, properties, and applications of graphene oxide/reduced graphene oxide and their nanocomposites. *Nano Mater Sci*. 2019. doi:10.1016/j.nanoms.2019.02.004

9. Foo ME, Gopinath SCB. Feasibility of graphene in biomedical applications. *Biomed Pharmacother*. 2017;94:354-361. doi:10.1016/j.biopha.2017.07.122

10. Gonçalves G, Marques P, Vila M. *Carbon Nanostructures Graphene-Based Materials in Health and Environment New Paradigms*.; 2016. http://www.springer.com/series/8633.

11. Depan D, Girase B, Shah JS, Misra RDK. Structure-process-property relationship of the polar graphene oxide-mediated cellular response and stimulated growth of osteoblasts on hybrid chitosan network structure nanocomposite scaffolds. *Acta Biomater*. 2011;7(9):3432-3445. doi:10.1016/j.actbio.2011.05.019

12. Ma L, Zhou M, He C, et al. Graphene-based advanced nanoplatforms and biocomposites from environmentally friendly and biomimetic approaches. *Green Chem*. 2019;21(18):4887-4918. doi:10.1039/c9gc02266j

13. Kudaibergenov S, Tatykhanova G, Bakranov N, Tursunova R. Layer-by-Layer Thin Films and Coatings Containing Metal Nanoparticles in Catalysis. *Thin Film Process - Artifacts Surf Phenom Technol Facet*. 2017. doi:10.5772/67215

14. Fatima M, Canhao H, Eurico J. Bone: A Composite Natural Material. *Adv Compos Mater - Anal Nat Man-Made Mater*. 2011. doi:10.5772/17523

15. Granito RN, Custódio MR, Rennó ACM. Natural marine sponges for bone tissue engineering: The state of art and future perspectives. *J Biomed Mater Res - Part B Appl Biomater*. 2017;105(6):1717-1727. doi:10.1002/jbm.b.33706

16. *Osteoporosis in Clinical Practice*. Springer London; 1998. doi:10.1007/978-1-4471-3382-7

17. Gonçalves GAB. NANOCOMPÓSITOS DE PMMA / HA / GRAFENO PARA APLICAÇÕES BIOMÉDICAS. 2012.

18. Iain H. Kalfas MDF. Principles of bone healing. *Neurosurg Focus*. 2001;10(4):1-4.

19. Alghazali KM, Nima ZA, Hamzah RN, Dhar MS, Anderson DE, Biris AS. Bone-tissue engineering: Complex tunable structural and biological responses to injury, drug delivery, and cell-based therapies. *Drug Metab Rev*. 2015;47(4):431-454. doi:10.3109/03602532.2015.1115871

20. Wang Q, Yan J, Yang J, Li B. Nanomaterials promise better bone repair. *Mater Today*. 2016;19(8):451-463. doi:10.1016/j.mattod.2015.12.003

21. Pires ALR, Bierhalz ACK, Moraes ÂM. Biomateriais: Tipos, aplicações e mercado. *Quim Nova*. 2015;38(7):957-971. doi:10.5935/0100-4042.20150094

22. Ahadian S, Rahal R, Ramón-Azcón J, Obregón R, Hasan A. Biomaterials in Tissue Engineering. *Tissue Eng Artif Organs Regen Med Smart Diagnostics Pers Med*. 2016;1-2:35-83. doi:10.1002/9783527689934.ch2

23. Bhatnagar I, Pallela R, Bramhachari PV, Ealla KKR. Chronicles of Sponge Biomaterials: The Saga in Biomedicine. *Mar Sponges Chem Biomed Appl*. 2016;(November):1-381. doi:10.1007/978-81-322-2794-6_15

24. Granito RN, Custódio MR, Rennó ACM. Natural marine sponges for bone tissue engineering: The state of art and future perspectives. *J Biomed Mater Res - Part B Appl Biomater*. 2017;105(6):1717-1727. doi:10.1002/jbm.b.33706

25. Wang D, Song J, Lin S, et al. A Marine-Inspired Hybrid Sponge for Highly Efficient Uranium Extraction from Seawater. *Adv Funct Mater*. 2019;29(32):1-12. doi:10.1002/adfm.201901009

26. Martins E, Rocha MS, Silva TH, Reis RL. *Remarkable Body Architecture of Marine Sponges as Biomimetic Structure for Application in Tissue Engineering*. Springer Singapore; 2019. doi:10.1007/978-981-13-8855-2_2

27. Wörheide G, Dohrmann M, Erpenbeck D, et al. *Deep Phylogeny and Evolution of Sponges (Phylum Porifera)*. Vol 61.; 2012. doi:10.1016/B978-0-12-387787-1.00007-6

28. Jesionowski T, Norman M, Zółtowska-Aksamitowska S, Petrenko I, Joseph Y, Ehrlich H. Marine spongin: Naturally prefabricated 3D scaffold-based biomaterial. *Mar Drugs*. 2018;16(3):1-23. doi:10.3390/md16030088

29. Zarrouk S, Ereskovsky A V., Mustapha K Ben, Abed A El, Pérez T. Sexual reproduction of hippospongia communis (lamarck, 1814) (dictyoceratida, demospongiae): Comparison of two populations living under contrasting environmental conditions. *Mar Ecol*. 2013;34(4):432-442. doi:10.1111/maec.12043

30. Norman M, Sc M. Poznan University of Technology PhD thesis Skeletons of selected marine demosponges as supports for dyes adsorption Supervisor : Professor Teofil Jesionowski. 2017.

31. Pallela R, Ehrlich H, Bhatnagar I. Biomedical Applications of Marine Sponge Collagens. *Mar Sponges Chem Biomed Appl*. 2016:1-381. doi:10.1007/978-81-

322-2794-6_20

32. Cell O, Oreffo ROC, Phil D. Natural Marine Sponge Fiber Skeleton : A Biomimetic Scaffold. 2003;9(6).

33. Naleway SE, Taylor JRA, Porter MM, Meyers MA, McKittrick J. Structure and mechanical properties of selected protective systems in marine organisms. *Mater Sci Eng C*. 2016;59:1143-1167. doi:10.1016/j.msec.2015.10.033

34. Saini R, Saini S, Sharma S. Nanotechnology: The future medicine. *J Cutan Aesthet Surg*. 2010;3(1):32. doi:10.4103/0974-2077.63301

35. Tudose IV, Koudoumas E, Pachiu C, et al. *Graphene-Based Materials and Their Biomedical and Environmental Applications: Recent Advances*. Elsevier Inc.; 2019. doi:10.1016/b978-0-12-814401-5.00009-8

36. Inagaki M, Kang F. *Engineering and Applications of Carbon Materials*.; 2014. doi:10.1016/b978-0-12-800858-4.00003-6

37. Aleksandrzak M, Urbas K. Nanomedical applications of graphene and graphene oxide. 2016;(May 2017). doi:10.5599/obp.9.21

38. Malgorzata Aleksandrzak*, Karolina Urbas, Magdalena Onyszko and EM. Biomedical applications of graphene and graphene oxide. *Acc Chem Res*. 2013;46(10):2211-2224. doi:10.1021/ar300159f

39. Zhu Y, Ji H, Cheng HM, Ruoff RS. Mass production and industrial applications of graphene materials. *Natl Sci Rev*. 2018;5(1):90-101. doi:10.1093/nsr/nwx055

40. Lin L, Peng H, Liu Z. Synthesis challenges for graphene industry. *Nat Mater*. 2019;18(6):520-524. doi:10.1038/s41563-019-0341-4

41. Ortiz Balbuena J, Tutor De Ureta P, Rivera Ruiz E, Mellor Pita S. Enfermedad de Vogt-Koyanagi-Harada. *Med Clin (Barc)*. 2016;146(2):93-94. doi:10.1016/j.medcli.2015.04.005

42. Backes C, Abdelkader A, Alonso C, et al. Production and processing of graphene and related materials To cite this version : HAL Id : hal-02144563 PRODUCTION AND PROCESSING OF GRAPHENE AND RELATED. 2019.

43. Shams SS, Zhang R, Zhu J. Graphene synthesis: A Review. *Mater Sci Pol*. 2015;33(3):566-578. doi:10.1515/msp-2015-0079

44. Novoselov KS, Fal'Ko VI, Colombo L, Gellert PR, Schwab MG, Kim K. A roadmap for graphene. *Nature*. 2012;490(7419):192-200. doi:10.1038/nature11458

45. Phiri J, Gane P, Maloney TC. General overview of graphene: Production, properties and application in polymer composites. *Mater Sci Eng B Solid-State Mater Adv Technol*. 2017;215:9-28. doi:10.1016/j.mseb.2016.10.004

46. Santos CIM, Gonçalves G, Cicuéndez M, et al. Biocompatible hybrids based on nanographene oxide covalently linked to glycolporphyrins: Synthesis, characterization and biological evaluation. *Carbon N Y*. 2018;135:202-214. doi:10.1016/j.carbon.2018.04.040

47. Ahmad N, Kausar A, Muhammad B. An investigation on 4-aminobenzoic acid modified polyvinyl chloride/graphene oxide and PVC/graphene oxide based nanocomposite membranes. *J Plast Film Sheeting*. 2016;32(4):419-448. doi:10.1177/8756087915616434

48. Pei S, Cheng HM. The reduction of graphene oxide. *Carbon N Y*. 2012;50(9):3210-3228. doi:10.1016/j.carbon.2011.11.010

49. O'Brien FJ. Biomaterials & scaffolds for tissue engineering. *Mater Today*. 2011;14(3):88-95. doi:10.1016/S1369-7021(11)70058-X

50. Bullock CJ, Bussy C. Biocompatibility Considerations in the Design of Graphene Biomedical Materials. *Adv Mater Interfaces*. 2019;6(11). doi:10.1002/admi.201900229

51. Duran M, Luzo ACM, de Souza JG, Favaro WJ, Garcia P, Duran N. Graphene Oxide as Scaffolds for Stem Cells: An Overview. *Curr Mol Med*. 2018;17(9):619-626. doi:10.2174/1566524018666180308111915

52. Fu C, Pan S, Ma Y, Kong W, Qi Z, Yang X. Effect of electrical stimulation combined with graphene-oxide-based membranes on neural stem cell proliferation and differentiation. *Artif Cells, Nanomedicine Biotechnol*. 2019;47(1):1867-1876. doi:10.1080/21691401.2019.1613422

53. Sladkova M, de Peppo GM. Bioreactor systems for human bone tissue engineering. *Processes*. 2014;2(2):494-525. doi:10.3390/pr2020494

54. Lewis JS, Barani Z, Magana AS, Kargar F. ce pte d M us pt. 2019:0-31.

55. Bordoni V, Reina G, Orecchioni M, et al. Stimulation of bone formation by monocyte-activator functionalized graphene oxide: In vivo. *Nanoscale*. 2019;11(41):19408-19421. doi:10.1039/c9nr03975a

56. Silva TH, Duarte ARC, Moreira-silva J. Examples of Natural and Nature-Inspired Materials. 1-Biomaterials from Marine-Origin Biopolymers. *Biomim Approaches Biomater Dev*. 2012;(1):1-22. https://www.facebook.com/%0Apapers3://publication/uuid/B34E0D5D-CB06-45B0-BE57-60E72462019D.

57. Lipton J, Weng GM, Röhr JA, Wang H, Taylor AD. Layer-by-Layer Assembly of Two-Dimensional Materials: Meticulous Control on the Nanoscale. *Matter*. 2020;2(5):1148-1165. doi:10.1016/j.matt.2020.03.012

58. Vallés C, Zhang X, Cao J, Lin F, Young RJ, Lombardo A. Graphene / Polyelectrolyte Layer-by-Layer Coatings for Electromagnetic Interference Shielding. :1-34.

59. Hong J, Han JY, Yoon H, et al. Carbon-based layer-by-layer nanostructures: From films to hollow capsules. *Nanoscale*. 2011;3(11):4515-4531. doi:10.1039/c1nr10575b

60. Oliveira DA, Gasparotto LHS, Siqueira JR. Processing of nanomaterials in layer-by-layer films: Potential applications in (bio)sensing and energy storage. *An Acad Bras Cienc*. 2019;91(2):1-17. doi:10.1590/0001-3765201920181343

61. Ariga K, Hill JP, Ji Q. Biomaterials and biofunctionality in layered macromolecular assemblies. *Macromol Biosci*. 2008;8(11):981-990. doi:10.1002/mabi.200800102

62. Yan X, Tao W, Cheng S, et al. Layer-by-layer assembly of bio-inspired borate/graphene oxide membranes for dye removal. *Chemosphere*. 2020;256:127118. doi:10.1016/j.chemosphere.2020.127118

63. Wang J, Wang H, Wang Y, Li J, Su Z, Wei G. Alternate layer-by-layer assembly of graphene oxide nanosheets and fibrinogen nanofibers on a silicon substrate

for a biomimetic three-dimensional hydroxyapatite scaffold. *J Mater Chem B*. 2014;2(42):7360-7368. doi:10.1039/c4tb01324g

64. Gangineni PK, Yandrapu S, Ghosh SK, Anand A, Prusty RK, Ray BC. Mechanical behavior of Graphene decorated carbon fiber reinforced polymer composites: An assessment of the influence of functional groups. *Compos Part A Appl Sci Manuf*. 2019;122(December 2018):36-44. doi:10.1016/j.compositesa.2019.04.017

65. Lee T, Min SH, Gu M, et al. Layer-by-Layer Assembly for Graphene-Based Multilayer Nanocomposites: Synthesis and Applications. *Chem Mater*. 2015;27(11):3785-3796. doi:10.1021/acs.chemmater.5b00491

66. Girão AF, Sousa J, Domínguez-Bajo A, et al. 3D Reduced Graphene Oxide Scaffolds with a Combinatorial Fibrous-Porous Architecture for Neural Tissue Engineering. *ACS Appl Mater Interfaces*. 2020;12(35):38962-38975. doi:10.1021/acsami.0c10599

67. Norman M, Bartczak P, Zdarta J, Ehrlich H, Jesionowski T. Anthocyanin dye conjugated with Hippospongia communis marine demosponge skeleton and its antiradical activity. *Dye Pigment*. 2016;134:541-552. doi:10.1016/j.dyepig.2016.08.019

68. Girão AF, Gonçalves G, Bhangra KS, et al. Electrostatic self-assembled graphene oxide-collagen scaffolds towards a three-dimensional microenvironment for biomimetic applications. *RSC Adv*. 2016;6(54):49039-49051. doi:10.1039/c6ra10213a

69. Zdarta J, Norman M, Smułek W, et al. Spongin-based scaffolds from Hippospongia communis demosponge as an effective support for lipase immobilization. *Catalysts*. 2017;7(5):1-20. doi:10.3390/catal7050147

70. Zdarta J, Antecka K, Frankowski R, Zgoła-Grześkowiak A, Ehrlich H, Jesionowski T. The effect of operational parameters on the biodegradation of bisphenols by Trametes versicolor laccase immobilized on Hippospongia communis spongin scaffolds. *Sci Total Environ*. 2018;615:784-795. doi:10.1016/j.scitotenv.2017.09.213

71. Norman M, Bartczak P, Zdarta J, et al. Sodium copper chlorophyllin immobilization onto Hippospongia communis marine demosponge skeleton and its antibacterial activity. *Int J Mol Sci*. 2016;17(10). doi:10.3390/ijms17101564

72. Szatkowski T, Siwínska-Stefánska K, Wysokowski M, et al. Immobilization of titanium(IV) oxide onto 3D spongin scaffolds of marine sponge origin according to extreme biomimetics principles for removal of C.I. basic blue 9. *Biomimetics*. 2017;2(2). doi:10.3390/biomimetics2020004

73. Hindryawati N, Maniam GP. Novel utilization of waste marine sponge (Demospongiae) as a catalyst in ultrasound-assisted transesterification of waste cooking oil. *Ultrason Sonochem*. 2015;22:454-462. doi:10.1016/j.ultsonch.2014.04.011

74. Zdarta J, Norman M, Smułek W, et al. Spongin-based scaffolds from Hippospongia communis demosponge as an effective support for lipase immobilization. *Catalysts*. 2017;7(5). doi:10.3390/catal7050147

75. Wulff JL. Resistance vs recovery: Morphological strategies of coral reef sponges. *Funct Ecol*. 2006;20(4):699-708. doi:10.1111/j.1365-2435.2006.01143.x

76. Zhang Y, Li R, Wu W, et al. Adhesion and Proliferation of Osteoblast-Like Cells on Porous Polyetherimide Scaffolds. *Biomed Res Int*. 2018;2018. doi:10.1155/2018/1491028

77. Zhang XZ, Zeng X, Sun YX, Zhuo RX. *Bioactive Materials in Gene Therapy*. Woodhead Publishing Limited; 2011. doi:10.1533/9780857092939.2.179

78. Valencia C, Valencia CH, Zuluaga F, Valencia ME, Mina JH, Grande-Tovar CD. Synthesis and application of scaffolds of chitosan-graphene oxide by the freeze-drying method for tissue regeneration. *Molecules*. 2018;23(10). doi:10.3390/molecules23102651

79. Johra FT, Jung WG. Hydrothermally reduced graphene oxide as a supercapacitor. *Appl Surf Sci*. 2015;357:1911-1914. doi:10.1016/j.apsusc.2015.09.128

80. Liu H, Kuila T, Kim NH, Ku BC, Lee JH. In situ synthesis of the reduced graphene oxide-polyethyleneimine composite and its gas barrier properties. *J Mater Chem A*. 2013;1(11):3739-3746. doi:10.1039/c3ta01228j

81. Liu C, Liu H, Lu C, Tang K, Zhang Y. Polyethyleneimine-modified graphene oxide/PNIPAm thermoresponsive hydrogels with rapid swelling/deswelling and improved mechanical properties. *J Mater Sci*. 2017;52(19):11715-11724. doi:10.1007/s10853-017-1301-5

82. Kamali M, Ghahremaninezhad A. A study of calcium-silicate-hydrate/polymer nanocomposites fabricated using the layer-by-layer method. *Materials (Basel)*. 2018;11(4). doi:10.3390/ma11040527

83. Yao H Bin, Wu LH, Cui CH, Fang HY, Yu SH. Direct fabrication of photoconductive patterns on LBL assembled graphene oxide/PDDA/titania hybrid films by photothermal and photocatalytic reduction. *J Mater Chem*. 2010;20(25):5190-5195. doi:10.1039/c0jm00094a

84. Jang SC, Hong SB, Yang HM, et al. Removal of radioactive cesium using prussian blue magnetic nanoparticles. *Nanomaterials*. 2014;4(4):894-901. doi:10.3390/nano4040894

85. Liu LJ, Gao X, Zhang P, et al. Ultrasensitive detection of ferulic acid using poly(diallyldimethylammonium chloride) functionalized graphene-based electrochemical sensor. *J Anal Methods Chem*. 2014;2014. doi:10.1155/2014/424790

86. Norman M, Bartczak P, Zdarta J, et al. Adsorption of C.I. natural red 4 onto spongin skeleton of marine demosponge. *Materials (Basel)*. 2015;8(1):96-116. doi:10.3390/ma8010096

87. Hu W, Peng C, Luo W, et al. Graphene-based antibacterial paper. *ACS Nano*. 2010;4(7):4317-4323. doi:10.1021/nn101097v

88. Jabbari F, Hesaraki S, Houshmand B. The physical, mechanical, and biological properties of silk fibroin/chitosan/reduced graphene oxide composite membranes for guided bone regeneration. *J Biomater Sci Polym Ed*. 2019;30(18):1779-1802. doi:10.1080/09205063.2019.1666235

89. Jia Z, Shi Y, Xiong P, et al. From Solution to Biointerface: Graphene Self-Assemblies of Varying Lateral Sizes and Surface Properties for Biofilm Control and Osteodifferentiation. *ACS Appl Mater Interfaces*. 2016;8(27):17151-17165. doi:10.1021/acsami.6b05198

90. Bandeiras C, Completo A, Ramos A, et al. Tissue Engineered Cartilage in Unconfined Compression: Biomechanical Analysis. *Mater Today Proc*. 2015;2(1):355-364. doi:10.1016/j.matpr.2015.04.032

91. Ciências DDE, Vida DA. Estudo da Actividade Biológica UNIVERSIDADE DE COIMBRA in vitro de Moléculas Fotossensibilizadoras para Terapia Fotodinâmica Estudo da Actividade Biológica in vitro de Moléculas Fotossensibilizadoras para Terapia Fotodinâmica Estudo da Actividade Biológic. 2014.

92. Liu H, Cheng J, Chen F, et al. Biomimetic and cell-mediated mineralization of hydroxyapatite by carrageenan functionalized graphene oxide. *ACS Appl Mater Interfaces*. 2014;6(5):3132-3140. doi:10.1021/am4057826

93. Carville NC, Collins L, Manzo M, et al. Biocompatibility of ferroelectric lithium niobate and the influence of polarization charge on osteoblast proliferation and function. *J Biomed Mater Res - Part A*. 2015;103(8):2540-2548. doi:10.1002/jbm.a.35390

94. Hazrin-Chong NH, Manefield M. An alternative SEM drying method using hexamethyldisilazane (HMDS) for microbial cell attachment studies on sub-bituminous coal. *J Microbiol Methods*. 2012;90(2):96-99. doi:10.1016/j.mimet.2012.04.014

95. Bai Y, Bai Y, Gao J, Ma W, Su J, Jia R. Preparation and characterization of reduced graphene oxide/fluorhydroxyapatite composites for medical implants. *J Alloys Compd*. 2016;688:657-667. doi:10.1016/j.jallcom.2016.07.006

96. Huang HY, Fan FY, Shen YK, et al. 3D poly-ε-caprolactone/graphene porous scaffolds for bone tissue engineering. *Colloids Surfaces A Physicochem Eng Asp*. 2020;606(May):125393. doi:10.1016/j.colsurfa.2020.125393

97. Holt BD, Wright ZM, Arnold AM, Sydlik SA. Graphene oxide as a scaffold for bone regeneration. *Wiley Interdiscip Rev Nanomedicine Nanobiotechnology*. 2017;9(3):1-18. doi:10.1002/wnan.1437

98. Kaspar D, Seidl W, Neidlinger-Wilke C, Claes L. In vitro effects of dynamic strain on the proliferative and metabolic activity of human osteoblasts. *J Musculoskelet Neuronal Interact*. 2000;1(2):161-164.

99. Simsikova M, Sikola T. Interaction of Graphene Oxide with Proteins and Applications of their Conjugates. *J Nanomedicine Res*. 2017;5(2):2-5. doi:10.15406/jnmr.2017.05.00109

100. Golzar H, Mohammadrezaei D, Yadegari A, et al. Incorporation of functionalized reduced graphene oxide/magnesium nanohybrid to enhance the osteoinductivity capability of 3D printed calcium phosphate-based scaffolds. *Compos Part B Eng*. 2020;185(March 2019):107749. doi:10.1016/j.compositesb.2020.107749

101. Zhao Y, Chen J, Zou L, Xu G, Geng Y. Facile one-step bioinspired mineralization by chitosan functionalized with graphene oxide to activate bone endogenous regeneration. *Chem Eng J*. 2019;378(July):122174. doi:10.1016/j.cej.2019.122174

102. Mohammadrezaei D, Golzar H, Rezai Rad M, et al. In vitro effect of graphene structures as an osteoinductive factor in bone tissue engineering: A systematic review. *J Biomed Mater Res - Part A*. 2018;106(8):2284-2343. doi:10.1002/jbm.a.36422

103. Gabbai-Armelin PR, Kido HW, Cruz MA, et al. Characterization and Cytotoxicity

Evaluation of a Marine Sponge Biosilica. *Mar Biotechnol*. 2019;21(1):65-75. doi:10.1007/s10126-018-9858-9

104. Skoda M, Dudek I, Szukiewicz D. Potential and Challenges of Graphene in Medicine. *Graphene based Mater Heal Environ*. 2016:3-33. doi:10.1007/978-3-319-45639-3_1

105. Wu X, Zheng S, Ye Y, Wu Y, Lin K, Su J. Enhanced osteogenic differentiation and bone regeneration of poly(lactic-: Co -glycolic acid) by graphene via activation of PI3K/Akt/GSK-3β/β-catenin signal circuit. *Biomater Sci*. 2018;6(5):1147-1158. doi:10.1039/c8bm00127h

106. Lopresti F, Maio A, Botta L, Scaffaro R. Preparation and mechanical characterization of polycaprolactone/graphene oxide biocomposite nanofibers. *AIP Conf Proc*. 2016;1736:1-5. doi:10.1063/1.4949680

107. Ryoo SR, Kim YK, Kim MH, Min DH. Behaviors of NIH-3T3 fibroblasts on graphene/carbon nanotubes: Proliferation, focal adhesion, and gene transfection studies. *ACS Nano*. 2010;4(11):6587-6598. doi:10.1021/nn1018279

108. Kim J, Choi KS, Kim Y, et al. Bioactive effects of graphene oxide cell culture substratum on structure and function of human adipose-derived stem cells. *J Biomed Mater Res - Part A*. 2013;101(12):3520-3530. doi:10.1002/jbm.a.34659

109. Li X, Lin K, Wang Z. Enhanced growth and osteogenic differentiation of MC3T3-E1 cells on Ti6Al4V alloys modified with reduced graphene oxide. *RSC Adv*. 2017;7(24):14430-14437. doi:10.1039/c6ra25832h

110. Lin Z, Solomon KL, Zhang X, et al. In vitro evaluation of natural marine sponge collagen as a scaffold for bone tissue engineering. *Int J Biol Sci*. 2011;7(7):968-977. doi:10.7150/ijbs.7.968